Article

Mechanistic Characterization of the HDV Genomic Ribozyme: Solvent Isotope Effects and Proton Inventories in the Absence of Divalent Metal Ions Support C75 as the General Acid

Andrea L. Cerrone-Szakal, Nathan A. Siegfried, and Philip C. Bevilacqua

J. Am. Chem. Soc., **2008**, 130 (44), 14504-14520 • DOI: 10.1021/ja801816k • Publication Date (Web): 09 October 2008

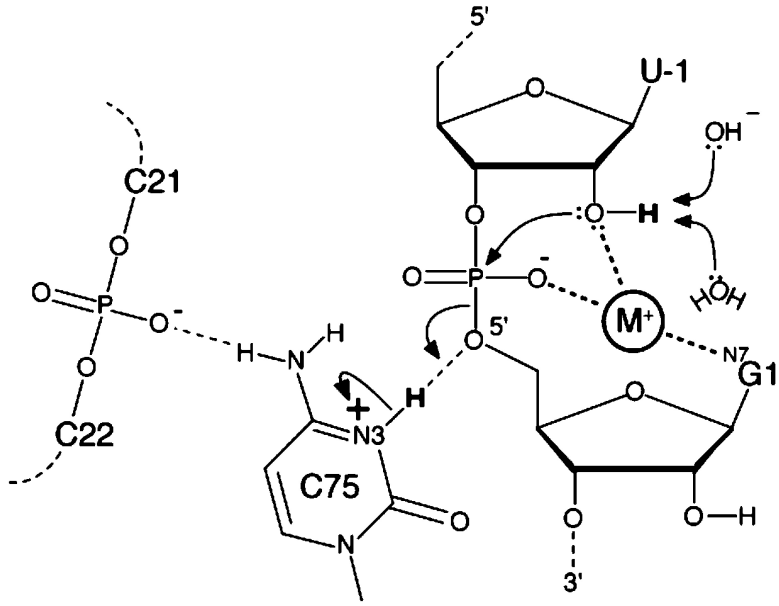

More About This Article

Additional resources and features associated with this article are available within the HTML version:

- Supporting Information
- Access to high resolution figures
- Links to articles and content related to this article
- Copyright permission to reproduce figures and/or text from this article

View the Full Text HTML

J|A|C|S
ARTICLES

Published on Web 10/09/2008

Mechanistic Characterization of the HDV Genomic Ribozyme: Solvent Isotope Effects and Proton Inventories in the Absence of Divalent Metal Ions Support C75 as the General Acid

Andrea L. Cerrone-Szakal,† Nathan A. Siegfried, and Philip C. Bevilacqua*

Department of Chemistry, The Pennsylvania State University, University Park, Pennsylvania 16802

Received March 11, 2008; E-mail: pcb@chem.psu.edu

Abstract: The hepatitis delta virus (HDV) ribozyme uses the nucleobase C75 and a hydrated Mg^{2+} ion as the general acid−base catalysts in phosphodiester bond cleavage at physiological salt. A mechanistic framework has been advanced that involves one Mg^{2+}-independent and two Mg^{2+}-dependent channels. The rate−pH profile for wild-type (WT) ribozyme in the Mg^{2+}-free channel is inverted relative to the fully Mg^{2+}-dependent channel, with each having a near-neutral pK_a. Inversion of the rate−pH profile was used as the crux of a mechanistic argument that C75 serves as general acid both in the presence and absence of Mg^{2+}. However, subsequent studies on a double mutant (DM) ribozyme suggested that the pK_a observed for WT in the absence of Mg^{2+} arises from ionization of C41, a structural nucleobase. To investigate this further, we acquired rate−pH/pD profiles and proton inventories for WT and DM in the absence of Mg^{2+}. Corrections were made for effects of ionic strength on hydrogen ion activity and pH meter readings. Results are accommodated by a model wherein the Mg^{2+}-free pK_a observed for WT arises from ionization of C75, and DM reactivity is compromised by protonation of C41. The Brønsted base appears to be water or hydroxide ion depending on pH. The observed pK_a's are related to salt-dependent pH titrations of a model oligonucleotide, as well as electrostatic calculations, which support the local environment for C75 in the absence of Mg^{2+} being similar to that in the presence of Mg^{2+} and impervious to bulk ions. Accordingly, the catalytic role of C75 as the general acid does not appear to depend on divalent ions or the identity of the Brønsted base.

Introduction

Overview of Nucleobase Catalysis. The ability of nucleobases to participate directly in RNA catalysis has become evident in recent years.[1] Although large ribozymes (>200 nt) such as the group I and II introns and RNase P require divalent metal ions for activity,[2−4] all five known small ribozymes (hammerhead, hairpin, VS, HDV, and glmS) function proficiently in high concentrations of EDTA and monovalent metal ions.[5−8] Quantitative dissection of the hammerhead and HDV ribozyme mechanisms revealed that divalent metal ions contribute only ∼10−25-fold to the rate of bond cleavage.[7,9,10]

These findings suggest that the primary role for divalent metal ions in small ribozymes is to drive folding, whereas bond breaking and making are facilitated by nondivalent metal ion mechanisms. Structural, biochemical, and computational studies on small ribozymes suggest that nucleobases can promote catalysis by hydrogen bonding in the transition state, stabilizing charge development via through-space interactions, and facilitating proton transfer as general acid−base catalysts, as summarized in ref 1. Despite this, the catalytic roles of particular ribozyme nucleobases in the absence of divalent ions are often poorly defined.

The HDV Ribozyme: Overview. The hepatitis delta virus (HDV) ribozyme is a small (∼85 nt), self-cleaving RNA that occurs in the genomic and antigenomic forms of the virus and is responsible for processing nascent viral transcripts to unit-length monomers during double rolling-circle replication.[11−13] A mammalian version of the HDV ribozyme has also been identified, which has structural and biochemical properties similar to those of the HDV ribozyme.[14]

† Present address: Center for Advanced Research in Biotechnology, University of Maryland Biotechnology Institute and the National Institute of Standards and Technology, 9600 Gudelsky Drive, Rockville, MD 20850.

(1) Bevilacqua, P. C.; Yajima, R. *Curr. Opin. Chem. Biol.* **2006**, *10*, 455–464.
(2) Hougland, J. L.; Kravchuk, A. V.; Herschlag, D.; Piccirilli, J. A. *PLoS Biol.* **2005**, *3*, 1536–1548.
(3) Stahley, M. R.; Strobel, S. A. *Science* **2005**, *309*, 1587–1590.
(4) Sigel, R. K.; Pyle, A. M. *Chem. Rev.* **2007**, *107*, 97–113.
(5) Murray, J. B.; Seyhan, A. A.; Walter, N. G.; Burke, J. M.; Scott, W. G. *Chem. Biol.* **1998**, *5*, 587–595.
(6) Nakano, S.; Chadalavada, D. M.; Bevilacqua, P. C. *Science* **2000**, *287*, 1493–1497.
(7) Nakano, S.; Proctor, D. J.; Bevilacqua, P. C. *Biochemistry* **2001**, *40*, 12022–12038.
(8) Roth, A.; Nahvi, A.; Lee, M.; Jona, I.; Breaker, R. R. *RNA* **2006**, *12*, 607–619.
(9) Curtis, E. A.; Bartel, D. P. *RNA* **2001**, *7*, 546–552.
(10) O'Rear, J. L.; Wang, S.; Feig, A. L.; Beigelman, L.; Uhlenbeck, O. C.; Herschlag, D. *RNA* **2001**, *7*, 537–545.
(11) Lai, M. M. *Annu. Rev. Biochem.* **1995**, *64*, 259–286.
(12) Wadkins, T. S.; Been, M. D. *Cell. Mol. Life Sci.* **2002**, *59*, 112–125.
(13) Been, M. D. *Curr. Top. Microbiol. Immunol.* **2006**, *307*, 47–65.
(14) Salehi-Ashtiani, K.; Luptak, A.; Litovchick, A.; Szostak, J. W. *Science* **2006**, *313*, 1788–1792.

10.1021/ja801816k CCC: $40.75

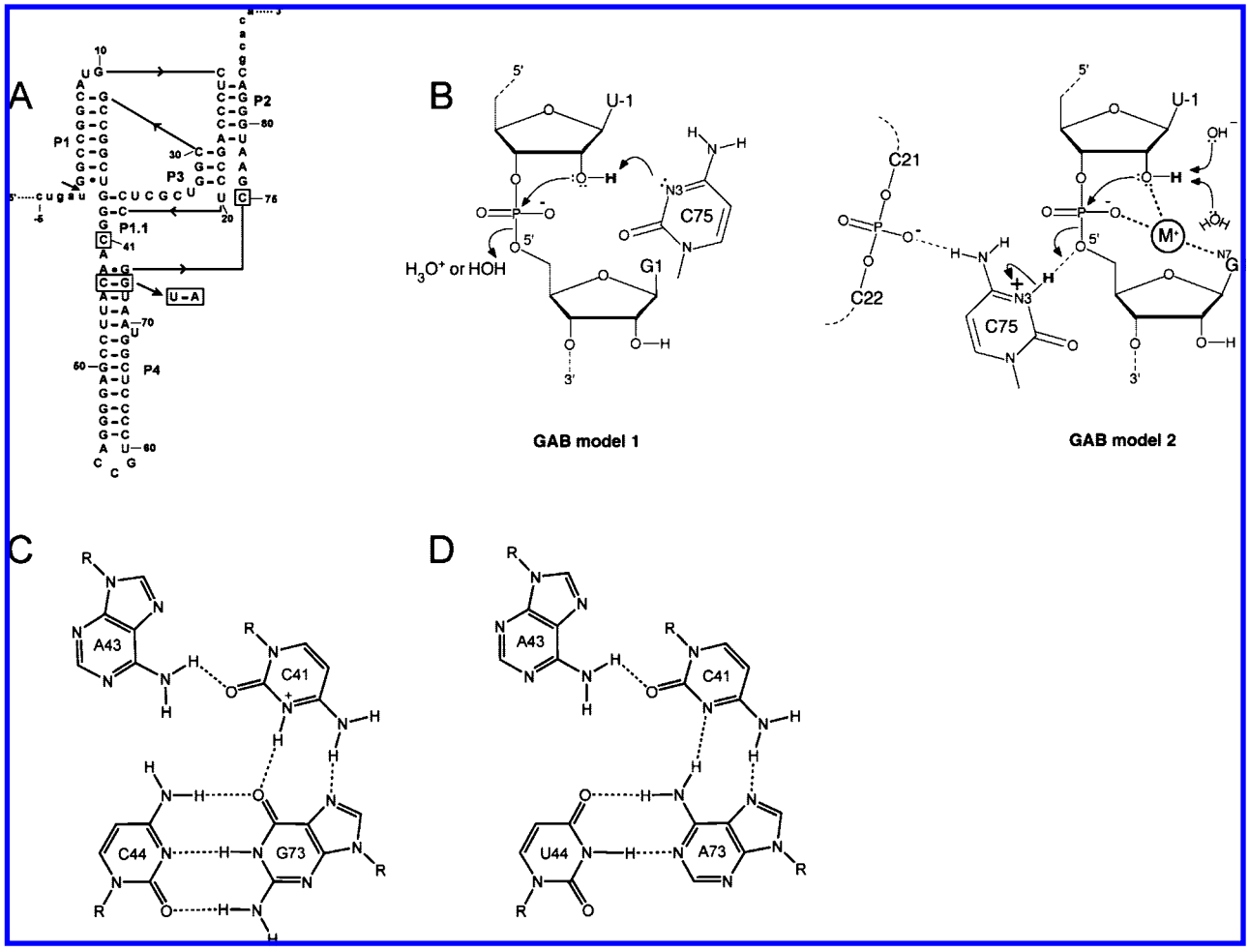

Figure 1. Sequence and structure for WT and DM HDV ribozymes. (A) Secondary structure of the ribozyme used in this study. The catalytic core is in uppercase, whereas the flanking sequence is in lowercase. Flanking sequence extends 30 nt upstream of the cleavage site (−30 position) and 15 nt downstream of P2 (99 position). The cleavage site between U-1 and G1 is denoted with an arrow; C41, the C44:G73 base pair of the base quadruple motif, and C75 are boxed. The site of the double mutation (CG to UA) in the base quadruple is indicated. The ribozyme has a G11C mutation (shown), which promotes fast, single-exponential kinetics (ref 45). (B) Proposed proton transfers in bond cleavage in the absence of divalent ions. Shown are both GAB model 1, in which C75 serves as the general base and water or hydronium ion serves as the Brønsted acid (left panel), and GAB model 2, in which protonated C75 serves as the general acid and water or hydroxide ion serves as the Brønsted base. The data herein provide stronger support for GAB model 2 as detailed in the text. Several explicit features of GAB model 2 are as follows. Either water or hydroxide ion can serve as the Brønsted base, depending on pH. Positioning of protonated C75 as the general acid is on the basis of biochemical studies conducted herein and previously (refs 6 and 24), as well as the structure of the cleaved form of the ribozyme which shows hydrogen bonding to the phosphate of C22 (ref 15). Placement of the monovalent ion in GAB model 2 is from a recent structure in Tl^+ ions, which reveals that a Tl^+ ion directly interacts with the 2′-OH of U-1, a nonbridging oxygen of the scissile phosphate, and the N7 of G1 (ref 18). A concerted one-step mechanism is shown for simplicity, but the reaction likely involves multiple steps as described in the text. (C) Hydrogen bonding of the bases in the WT base quadruple motif (ref 16). (D) Hydrogen bonding of the bases in the DM base quadruple motif, in which the C44:G73 base pair has been changed to a U:A, as described (refs 19 and 34).

The HDV ribozymes have secondary structures that comprise five pairing regions that together form a nested double pseudoknot (Figure 1A). Crystal structures of product and precleaved forms of the ribozyme have been solved, most recently in the presence of thallium ions (Tl^+).[15−18] These structures reveal a solvent-excluded catalytic core with C75 positioned to partake in catalysis.

The ribozyme uses the 2′-OH of U-1 as a nucleophile to cleave the phosphodiester bond between nucleotides −1 and +1, yielding products with 5′-OH and 2′,3′-cyclic phosphate termini (Figure 1B). Although the HDV ribozyme can react in the absence of divalent ions, assured by high concentrations of EDTA, a hydrated divalent ion appears to contribute to the self-cleavage mechanism under physiological conditions by serving both folding and general acid−base roles as described below.[6,7,19] Although many divalent ions can facilitate HDV ribozyme catalysis at similar levels, (e.g., Mg^{2+}, Ca^{2+}, Sr^{2+}, Ba^{2+}, Mn^{2+}, and Co^{2+}) the divalent ion that has received the greatest attention is Mg^{2+}.[20,21] It is also well established that C75[22] participates in the reaction as a general acid−base catalyst.[6,15,23,24]

(15) Ferre-D'Amare, A. R.; Zhou, K.; Doudna, J. A. *Nature* **1998**, *395*, 567–574.
(16) Ferre-D'Amare, A. R.; Doudna, J. A. *J. Mol. Biol.* **2000**, *295*, 541–556.
(17) Ke, A.; Zhou, K.; Ding, F.; Cate, J. H.; Doudna, J. A. *Nature* **2004**, *429*, 201–205.
(18) Ke, A.; Ding, F.; Batchelor, J. D.; Doudna, J. A. *Structure* **2007**, *15*, 281–287.
(19) Wadkins, T. S.; Shih, I.; Perrotta, A. T.; Been, M. D. *J. Mol. Biol.* **2001**, *305*, 1045–1055.
(20) Suh, Y. A.; Kumar, P. K.; Taira, K.; Nishikawa, S. *Nucleic Acids Res.* **1993**, *21*, 3277–3280.

The HDV Ribozyme: Dependence on pH. A number of mechanistic investigations of the HDV ribozyme have been performed. Many of these studies have focused on the pH dependence of the ribozyme reaction in an effort to explain the number and affinity of various structural and catalytic protonations. These types of experiments can have various complications associated with them such as changes in rate-limiting step with pH and misfolding of the ribozyme. It is therefore important to consider the relevant literature.

The initial data implicating C75 in proton transfer came from the crystal structure of the self-cleaved ribozyme, which showed the N3 of C75 positioned within hydrogen-bonding distance of the leaving group 5′-oxygen of G1.[15,16] Consistent with an important role in the mechanism, a C75U mutation rendered the ribozyme inactive both in the presence and absence of divalent ions.[6,23] Been and co-workers demonstrated that the catalytically inactive C75U and C75Δ ribozymes can be rescued by addition of exogenous imidazole, supporting a histidine-like role for C75 in proton transfer.[23,25] Rate−pH profiles in the presence of Mg^{2+} revealed a low-pH arm with a slope of 1, consistent with one proton transfer occurring in the rate-limiting step of the reaction, and a plateau in the high-pH region, which together provided an observed pK_a near neutrality.[6,23] A number of functional studies support the assignment of this pK_a to C75,[6,23−27] including a recent study in which the pK_a of C75 was directly measured using Raman crystallography.[28]

When ribozyme self-cleavage reactions are performed in D_2O, a substantial kinetic solvent isotope effect (KSIE) is observed over the entire experimental pH 4−9 range,[6,25,29] with a KSIE of ∼4-fold in the plateau range, suggesting that proton transfer occurs in the rate-limiting step of the reaction. Tinsley et al.[30] pointed out that conformational changes, in addition to chemistry, have the potential to contribute to observed solvent isotope effects in the HDV ribozyme and that this possibility can be tested by examining the shape of proton inventories (see the Discussion). In addition, the observed pK_a shifts upward by ∼0.4[6,29] to 0.7[25] units in D_2O, consistent with proton transfer involving the ring nitrogen of a cytosine.[31−33]

Been and co-workers have shown for both the antigenomic and genomic ribozymes that the rate of the reaction depends log−linearly on the pK_a of the small molecule used in rescue, with a slope of 0.47 and a good R value for the fit. These studies provide strong support for C75 in proton transfer, as opposed to a purely electrostatic or structural role which would give a slope of zero.[25,27] These activity rescue experiments used small-molecule nucleobase or imidazole derivatives at their pH optima, with pK_a values ranging over nearly 4 logs (pK_a of ∼4 to ∼8). The small-molecule derivatives differed enough in structure to suggest that structural factors do not appreciably perturb the relationship and, therefore, that the keto and amine groups on C do not play important roles, at least when delivered exogenously.

Scheme 1. Three-Channel Mechanism for Ribozyme Cleavage[a,b,c]

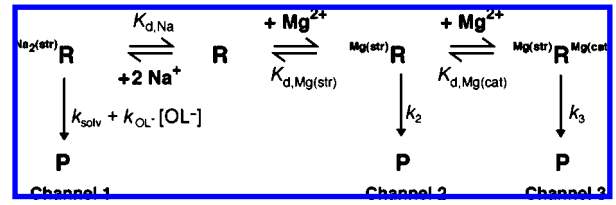

Scheme 2. Double-Subchannel/Single-Protonation Mechanism

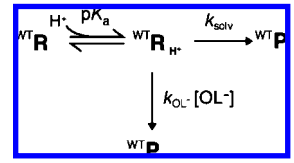

Scheme 3. Single-Channel/Single-Deprotonation Mechanism

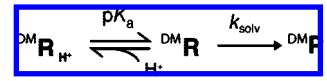

[a] Each scheme is named on the basis of the number of protonation/deprotonation events necessary to go from the ribozyme species furthest from the reactive state to the reactive state. In addition, "WT" and "DM" are used within a given scheme to indicate the ribozyme to which the scheme applies. [b] States are shown with protium as the isotope for simplicity, but they can be deuterium or a mixture of protium and deuterium depending on the composition of the solvent. [c] Channel 1 subchannels and protonation events, depicted explicitly in Schemes 2−4, are important for Scheme 1/channel 1 as well, but most details are omitted from Scheme 1 for clarity.

The HDV Ribozyme: Dependence on Mg^{2+}. Studies of the metal ion dependence of the genomic HDV ribozyme led to a framework in which the ribozyme can self-cleave by one Mg^{2+}-independent and two Mg^{2+}-dependent channels (Scheme 1).[7,21,34] Channel 1 of Scheme 1 involves cleavage in the absence of divalent metal ions and consists of solvent- and hydroxide-catalyzed subchannels, as illustrated in Scheme 2 and described below. Channel 2 involves cleavage in the presence of a structural Mg^{2+} ion, whereas channel 3 involves cleavage in the presence of structural *and* catalytic Mg^{2+} ions.

The primary evidence supporting the presence of these three channels comes from extensive rate−Mg^{2+} studies, which were conducted parametrically in pH.[7] We note that these studies were performed in metal-buffered solutions to allow very low (nanomolar) concentrations of free Mg^{2+} to be accessed, all in the background of 1 M NaCl to aid RNA folding. Changes in the rate−pH profiles were consistent with participation of a metal ion in general acid−base chemistry *only* when free Mg^{2+} concentrations exceeded ∼1 mM (Channel 3). However, Mg^{2+} was found to assist the observed rate at concentrations above ∼0.1 μM which supported Channel 2 with a structural Mg^{2+} ion. The quantitative contributions of Mg^{2+} to channels 2 and 3 were calculated at ∼125- and ∼25-fold, respectively; of

(21) Nakano, S.; Cerrone, A. L.; Bevilacqua, P. C. *Biochemistry* **2003**, *42*, 2982–2994.
(22) In the antigenomic version of the ribozyme the catalytic cytosine is numbered as C76 rather than C75. We refer to this catalytic cytosine as simply "C75" throughout the study.
(23) Perrotta, A. T.; Shih, I.; Been, M. D. *Science* **1999**, *286*, 123–126.
(24) Das, S. R.; Piccirilli, J. A. *Nat. Chem. Biol.* **2005**, *1*, 45–52.
(25) Shih, I. H.; Been, M. D. *Proc. Natl. Acad. Sci. U.S.A.* **2001**, *98*, 1489–1494.
(26) Oyelere, A. K.; Kardon, J. R.; Strobel, S. A. *Biochemistry* **2002**, *41*, 3667–3675.
(27) Perrotta, A. T.; Wadkins, T. S.; Been, M. D. *RNA* **2006**, *12*, 1282–1291.
(28) Gong, B.; Chen, J. H.; Chase, E.; Chadalavada, D. M.; Yajima, R.; Golden, B. L.; Bevilacqua, P. C.; Carey, P. R. *J. Am. Chem. Soc.* **2007**, *129*, 13335–13342.
(29) Nakano, S.; Bevilacqua, P. C. *J. Am. Chem. Soc.* **2001**, *123*, 11333–11334.
(30) Tinsley, R. A.; Harris, D. A.; Walter, N. G. *J. Am. Chem. Soc.* **2003**, *125*, 13972–13973.
(31) Schowen, K. B.; Schowen, R. L. *Methods Enzymol.* **1982**, *87*, 551–606.
(32) Shim, J. H.; Benkovic, S. J. *Biochemistry* **1999**, *38*, 10024–10031.
(33) Luptak, A.; Ferre-D'Amare, A. R.; Zhou, K.; Zilm, K. W.; Doudna, J. A. *J. Am. Chem. Soc.* **2001**, *123*, 8447–8452.
(34) Nakano, S.; Bevilacqua, P. C. *Biochemistry* **2007**, *46*, 3001–3012.

particular note is that divalent ions contributes quite modestly to chemistry at just ~25-fold.

Channel 1 of Scheme 1 is of interest to the present study. It describes uptake of at least two sodium ions, as supported by the slope of a log k_{obs}−log[NaCl] plot,[21] and contains solvent- and hydroxide-catalyzed subchannels and a C75 protonation event, as described herein and depicted explicitly in Schemes 2−4. Additional studies suggested that the catalytic ion binds via outer-sphere-like coordination,[6,21] whereas the structural metal ion binds via inner-sphere coordination.[21] Several observations from biochemical studies support a catalytic metal ion interaction at the active site: (1) binding of the catalytic H^+ and the catalytic Mg^{2+} is anticooperative both in solution and in the crystal, suggesting their binding sites are proximal,[6,28,34] (2) switching the scissile phosphate linkage from 3′−5′ to 2′−5′ alters the metal preference of the reaction,[35] (3) changing the identity of the −1 nucleotide affects the metal ion preference of the reaction,[36] and (4) changing the G·U wobble pair at the base of P1 modestly alters the metal-binding characteristics of the reaction.[37]

The HDV Ribozyme: Two Models for Catalysis by C75. Two models have been advanced for how C75 and Mg^{2+} contribute to general acid−base catalysis, as recently summarized in ref 34 and depicted in Figure 1B. In general acid−base model 1 (GAB model 1), C75 acts as a general base to deprotonate the 2′-OH of U-1; the Brønsted acid in the presence of Mg^{2+} is proposed to be a hydrated Mg^{2+} ion, and in the absence of Mg^{2+} could be water or a hydronium ion (Figure 1B). This model is supported by recent crystal structures, as well as molecular dynamics studies of the precleaved state.[17,38−40]

In general acid−base model 2 (GAB model 2), a mechanism that swaps the general acid and base roles is proposed. Protonated C75H$^+$ acts as a general acid; the Brønsted base in the presence of Mg^{2+} is proposed to be a hydrated Mg^{2+} hydroxide ion and in the absence of Mg^{2+} could be water or a hydroxide ion (Figure 1B). GAB model 2 in the presence of Mg^{2+} is supported by several biochemical and physical organic studies,[6,7,24] as well as theoretical studies by density functional theory (DFT)[41] and quantum mechanics−molecular mechanics (QM−MM),[42] albeit these calculations are based on structural models that at present do not contain the scissile phosphate.

Of particular importance to supporting GAB model 2 is a study by Das and Piccirilli in the *presence of Mg^{2+}* in which the 5′-bridging oxygen leaving group in the antigenomic HDV ribozyme reaction was replaced with sulfur to give a 5′-phosphorothiolate. This mutation changes the character of the leaving group from poor to excellent such that it no longer needs to be protonated to leave. Remarkably, the 5′-phosphorothiolate suppressed the deleterious effect that C76U and 3-deazacytosine (c3C) substitutions have on ribozymes with the natural 5′-oxygen leaving group and restored ribozyme activity to near WT levels under certain conditions. This finding directly associates a protonated N3 of C76 (and thus C75 in the genomic ribozyme) with protonation of the leaving group in the Mg^{2+}-dependent cleavage reaction.[24] This incisive experiment parallels a study on RNase A that assigned general acid and base roles in RNA cleavage to specific histidine residues.[43] The catalytic role of C75 in the *absence of divalent ions*, however, is not well defined. One suggestion is that C75 could be either the general acid *or* the general base, with its role depending on the reaction conditions or HDV construct used.[40]

Mechanistic experiments have been performed in the absence of divalent ions. In the presence of high EDTA and monovalent metal ion concentrations (channel 1) as well as submillimolar Mg^{2+} concentrations and high monovalent metal ion concentrations (channel 2), the rate−pH profiles of the genomic and antigenomic ribozymes are inverted relative to those in higher Mg^{2+} concentrations: the channel 1 and 2 rate−pH profiles have a plateau region at low pH and an arm with a slope of −1 between pH 6 and 8.[6,7,19] This observation was used as the basis for early mechanistic arguments that C75 participates in the reaction as a general acid.[6] This interpretation was to be questioned, however, because reactions of mutant ribozymes were found to be independent of pH in the absence of Mg^{2+}.[19]

The HDV Ribozyme: Effects of a C41 Double Mutant. In WT, protonated C41 engages in a base quadruple motif, as first identified in structural studies (Figure 1C).[15,16] Biochemical support for protonation of C41 came from kinetic and thermal denaturation studies of a double mutant (DM) HDV genomic ribozyme with a C44U:G73A change, which allows the base quadruple to form without C41 protonation (Figure 1D).[19,34] The rate of DM in the absence of divalent metal ions was found to be independent of pH, suggesting that the divalent ion-free pK_a observed for WT is for ionization of C41 rather than C75.[19] Moreover, deleting nucleotides 41−43 in the WT background, which removes the base quadruple motif altogether (Figure 1), also eliminated the pH dependence of the reaction. Although it was later demonstrated by nucleotide analogue interference mapping (NAIM)[26] and nucleobase rescue experiments[27] that C41 does not play a direct catalytic role in the HDV ribozyme mechanism in the presence of Mg^{2+}, it remained possible that ionization of C41 could indirectly influence the pH dependence of WT in the absence of divalent ions.

In an attempt to help understand the rate−pH profile inversion for the HDV ribozyme, we probed the nature of the rate-limiting step for WT and DM in the absence of divalent metal ions using KSIE and proton inventory experiments. Results are best accommodated by a model in which the pK_a observed for WT is due to ionization of C75, whereas the pK_a observed for DM is due to protonation of C41 resulting in a non-native base quadruple. According to this model, inversion of the rate−pH profile for the WT upon removal of the catalytic divalent ion supports a mechanism with C75 as the general acid both in the presence and absence of divalent ions.

Materials and Methods

Abbreviations Used. AS(−30/−7), antisense oligonucleotide targeted to the −30 to −7 stretch upstream of the self-cleavage site between −1 and +1; C41, nucleobase that engages in a base triple with A43 and G73, that together with C44 is referred to as "the base quadruple motif"; DM, double mutant in the background of the monophasic, fast-reacting G11C change in which C44 and

(35) Shih, I. H.; Been, M. D. *RNA* **1999**, *5*, 1140–1148.
(36) Perrotta, A. T.; Been, M. D. *Biochemistry* **2007**, *46*, 5124–5130.
(37) Cerrone-Szakal, A. L.; Chadalavada, D. M.; Golden, B. L.; Bevilacqua, P. C. *RNA* **2008**, *14*, 1746–1760.
(38) Krasovska, M. V.; Sefcikova, J.; Réblová, K.; Schneider, B.; Walter, N. G.; Šponer, J. *Biophys. J.* **2006**, *91*, 626–638.
(39) Krasovska, M. V.; Sefcikova, J.; Špačková, N.; Šponer, J.; Walter, N. G. *J. Mol. Biol.* **2005**, *351*, 731–748.
(40) Banáš, P.; Rulíšek, L.; Hánošová, V.; Svozil, D.; Walter, N. G.; Šponer, J.; Otyepka, M. *J. Phys. Chem. B* **2008**, *112*, 11177–11187.
(41) Liu, H.; Robinet, J. J.; Ananvoranich, S.; Gauld, J. W. *J. Phys. Chem. B* **2007**, *111*, 439–445.
(42) Wei, K.; Liu, L.; Cheng, Y. H.; Fu, Y.; Guo, Q. X. *J. Phys. Chem. B* **2007**, *111*, 1514–1516.
(43) Thompson, J. E.; Raines, R. T. *J. Am. Chem. Soc.* **1994**, *116*, 5467–5468.

G73 of the C41 base quadruple motif are changed to a U and an A, respectively; EDTA, ethylenediaminetetraacetic acid; GAB model 1, general acid−base model for cleavage in which C75 acts as the general base; GAB model 2, general acid−base model for cleavage in which $C75H^+$ acts as the general acid; HDV, hepatitis delta virus; OL^-, lyoxide ion, which is either OH^- or OD^-, depending on solvent composition; pK_a, K_a is an acid dissociation constant; k_{obs}, observed rate constant for self-cleavage; KSIE, kinetic solvent isotope effect; n, the mole fraction of D_2O in solution; nt, nucleotide; pL, pH or pD; WT, wild-type ribozyme, which is in the background of the fast-reacting, monophasic G11C change; ϕ^E, equilibrium fractionation factor, which allows the equilibrium isotope effect of K_H/K_D to be calculated from $K_H/K_D = 1/\phi^E$; ϕ^T, transition state fractionation factor, which describes the deuterium preference of a particular site relative to that of an average bulk-water molecule.

Chemicals. Ultrapurified deionized water (H_2O) (Barnstead NANOpure DIamond Water Purification Systems) was used for all sample preparations that involved H_2O. Deuterium oxide (D_2O) (D, 99.9%) (Cambridge Isotope Laboratories) was used for all sample preparations that involved D_2O. A synthetic DNA antisense oligonucleotide, AS(−30/−7),[44] was purchased from Integrated DNA Technologies (IDT) and used without further purification.

Preparation of RNA and Buffers. The −30/99 genomic HDV RNA used here was transcribed from pT7 −30/99 using phage T7 polymerase as described.[44] This transcript contains 30 nt upstream of the cleavage site and 15 nt downstream of the 3′ end of the ribozyme. All transcripts contain a G11C mutation that biases the equilibrium between Alt P1 and P1 toward the native fold.[45] Transcripts were *Bfa* I run-offs that contain ribozyme and HDV-derived RNA sequence only. RNA was transcribed, purified, and 5′-end-radiolabeled as described.[44] All mutant plasmids were generated from pT7 −30/99 using the QuikChange kit (Stratagene). Sequences were confirmed by dideoxy sequencing after both minipreps and maxipreps (Qiagen). The ribozyme with the G11C change is referred to as wild-type (WT). The ribozyme with the G11C change and the base quadruple motif mutations is referred to as double mutant (DM).

5′-end-radiolabeled RNA was dissolved in H_2O, and split into two aliquots. One aliquot was dried and resuspended in D_2O, and this process was repeated to ensure that all H_2O was removed. All reactions contained AS(−30/−7),[44] stock solutions of which were prepared using H_2O and D_2O as described for the ribozyme.

The buffer was 25 mM MES for experiments at pL 5.5−6.9 and 25 mM HEPES for experiments at pL 6.9−9.7. The following stock solutions were prepared: 2× ME (50 mM MES/200 mM Na_2EDTA), 2× HE (50 mM HEPES/200 mM Na_2EDTA), 1.2× MEN (25 mM MES/100 mM Na_2EDTA/1.2 M NaCl), and 1.2× HEN (25 mM HEPES/100 mM Na_2EDTA/1.2 M NaCl). The buffers were prepared by dissolving the appropriate salts in H_2O or D_2O. Buffers in H_2O were adjusted to the desired pL value using 1−4 M HCl or NaOH prepared with H_2O, whereas D_2O buffers were adjusted to the desired pL values using 1−4 M HCl or NaOH prepared with D_2O. Measurements of pL values were at 37 °C, the same temperature at which the reaction was conducted. Meter readings were adjusted to pH as described below. For the reactions in D_2O, the pD was determined by adding 0.4 to the corrected pH meter reading.[31]

Ribozyme Kinetics and Data Fitting. Reactions were performed similarly to previously described.[6,7] A typical self-cleavage reaction contained 2 nM 5′-end-radiolabeled RNA, 25 mM buffer, 100 mM Na_2EDTA, 10 μM AS(−30/−7), and 1 M NaCl. (Considerations for choosing 1 M as the working NaCl concentration and 100 mM as the working EDTA concentration are presented in the Results.) The RNA was renatured at 55 °C for 10 min in the presence of AS(−30/−7) and H_2O or D_2O as appropriate, then cooled at room temperature for 10 min. Renatured RNA was diluted with an equal volume of 2× ME or 2× HE buffer, and the mixture was incubated at 37 °C for 2 min. A zero time-point was removed and self-cleavage was initiated by the addition of an appropriate volume of 1.2× MEN or 1.2× HEN buffer. All time-points were quenched by mixing with an equal volume of 95% (v/v) formamide loading buffer (no EDTA) and immediately placing on dry ice. All reactions were performed for a total of 48 h. At the end of each reaction in H_2O, the pH of the mixture was checked with pH paper to confirm that the correct pH was maintained throughout the reaction. Time-points were fractionated on a denaturing 10% (w/v) polyacrylamide gel. Gels were dried and visualized using a PhosphorImager (Molecular Dynamics).

Plots of fraction product versus time were constructed. Most WT ribozyme reactions could be fit to a single-exponential equation (eq 1), where f is the fraction of ribozyme cleaved, A is the fraction of ribozyme cleaved at completion (usually ∼80%), $A + B$ is the burst fraction (in all cases herein, $A + B \approx 0$), k_{obs} is the observed first-order rate constant, and t is time.

$$f = A + Be^{-k_{obs}t} \quad (1)$$

Parameters were obtained using nonlinear least-squares fitting by KaleidaGraph (Synergy Software). Typically, 3−6 half-lives of data were collected.

For the WT ribozyme reactions at pL ∼ 9−10 and most of DM reactions, plots of fraction product versus time were linear, representing the early portion of an exponential time course. At early time, eq 1 reduces to eq 2:

$$f_{early} = Ak_{obs}t \quad (2)$$

Such plots were fit to eq 3 where m, the slope of the line, is Ak_{obs}:

$$f_{early} = mt + b \quad (3)$$

k_{obs} was obtained by dividing m by A, which was assumed to be 80% on the basis of time courses that could be fit using eq 1.

The pL ∼ 5.5, 6.5, 7.5, 8.7, and 9.7 data points in each rate−pL profile were performed in duplicate and on different days, and nearly the same rates were obtained in all cases, providing confidence in the rate−pL profiles reported here.

In general, the equations used to fit the rate−pL profiles were derived from schemes involving the minimal number of protonation or deprotonation events necessary to arrive at the active ribozyme species. The log rate−pH profiles for WT were fit according to the logarithm of eq 4, which was derived from the double-subchannel/single-protonation mechanism shown in Scheme 2:

$$k_{obs,HOH} = \frac{k_{HOH} + k_{OH^-}10^{pH-pK_{HOH}}}{1 + 10^{pH-pK_{R,H}}} \quad (4)$$

where pK_{HOH} is the autoprotolysis constant (pK_w) of H_2O and p$K_{R,H}$ is the pK_a of the titratable group on the ribozyme in the presence of H_2O. At 1 M ionic strength and 37 °C, the pK_w of H_2O is reported as 13.38.[31] At high pH, eq 4 has the pH-independent limit, $k_{obs,HOH} = k_{OH^-}10^{pK_{R,H}-pK_{HOH}}$, which arises because of compensation between decrease in the concentration of the putative general acid (protonated C75) with pH and increase in the concentration of the putative Brønsted base (hydroxide ion) with pH. Because the autoprotolysis constant used in the present study is corrected for ionic strength, the value for k_{OH^-} differs slightly more than expected from an earlier study, which assumed a standard value pK_w of 14 (see the Results and Table 1).

According to Scheme 2, the ribozyme is active when protonated, which allows it to react via two subchannels. In one subchannel, solvent participates as the Brønsted base, with rate constant k_{solv} (either k_{HOH} or k_{DOD} in pure H_2O or D_2O, respectively), while in the other subchannel lyoxide ion participates as the Brønsted base, with a pseudo-first-order rate constant of $k_{OL^-}[OL^-]$ (Figure 1B). Specific base catalysis by lyoxide ion is inferred from both the high-

(44) Chadalavada, D. M.; Knudsen, S. M.; Nakano, S.; Bevilacqua, P. C. *J. Mol. Biol.* **2000**, *301*, 349–367.
(45) Chadalavada, D. M.; Senchak, S. E.; Bevilacqua, P. C. *J. Mol. Biol.* **2002**, *317*, 559–575.

Table 1. pK_a Values from This and Previous Studies of the HDV Ribozyme[a]

conditions	WT (in H_2O)	WT (in D_2O)	DM (in H_2O)	DM (in D_2O)
	C75 pK_a Values			
no bound Mg^{2+} (channel 3)[b]	7.25[c]	ND	7.25[c,d]	ND
0.87 mM Mg^{2+} (channel 3)	7.1[e,f]	7.4[f]	7.1[c,d]	ND
10 mM Mg^{2+} (channel 3)	6.1[e,f]	6.5[f,g]	6.1[c,d]	ND
bound Mg^{2+} (channel 3)[b]	5.9[c]	ND	5.9[c,d]	ND
1 M NaCl/100 mM Na_2EDTA (channel 1)	7.25[h,i,j] **7.48 ± 0.07**[k]	**7.92 ± 0.08**[k]	NP	NP
	C41 pK_a Values			
no bound Mg^{2+} (channel 2)[b]	5.5[c]	ND	ND	ND
0.87 mM Mg^{2+} (channel 3)	ND	ND	5.7[c,d]	ND
10 mM Mg^{2+} (channel 3)	ND	ND	5.6[c,d]	ND
bound Mg^{2+} (channel 2)[b]	7.1[c]	ND	ND	ND
1 M NaCl/100 mM Na_2EDTA (channel 1)	NP	NP	6.45[c,j] **6.32 ± 0.03**[k]	**6.76 ± 0.03**[k]

[a] Values determined in this study are in bold type. Errors in previously reported pK_a values were ±0.1−0.3. Errors determined in the present study are provided in the table. [b] These values are from extrapolations to Mg^{2+}-free and -bound states of the ribozyme. [c] Ref 34. [d] Two pK_a values were observed for DM under these conditions. The higher value was assigned to C75, and the lower value to C41, whose protonation induces inactivation of the DM (ref 34). [e] These values are from kinetic studies in solution and Raman studies on crystals and are in good agreement (refs 6 and 28). [f] Ref 29. [g] Slightly larger (+0.7 units) D_2O shifts were reported elsewhere (ref 25). [h] Ref 7. [i] A second (lower) value of 5.6 was present in some of the fits but found herein only in the presence of rate−pD plots (Figure 2A). [j] Previously reported values in 1 M NaCl have been corrected upward by 0.60 and 0.65, respectively, according to 1.2 M NaCl meter calibrations. [k] Values determined in this study. Assignment of these pK_a values to C75 or C41 is on the basis of analysis described in the text. ND = not determined; NP = pK_a not present in these data sets.

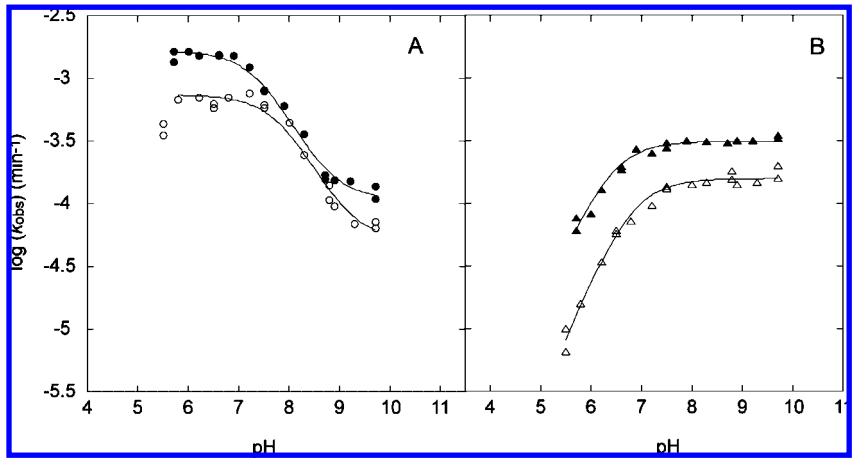

Figure 2. Comparison of rate−pL profiles for WT and DM in the absence of divalent ions (in 1 M NaCl, 100 mM EDTA) in H_2O (filled symbols) and D_2O (open symbols). Both plots share the same *y*-axis in order to facilitate comparison. (A) The rate−pH profile for the WT ribozyme was fit according to the logarithm of eq 4 ($R^2 > 0.99$), and the following parameters were obtained: $k_{HOH} = 1.66\ (\pm 0.09) \times 10^{-3}\ min^{-1}$, $k_{OH^-} = 86 \pm 18\ M^{-1}\ min^{-1}$, and p$K_a$ = 7.48 ± 0.07. The rate−pD profile, excluding the lowest pD value, for the WT ribozyme was fit according to the logarithm of eq 5 ($R^2 = 0.99$), and the following parameters were obtained: $k_{DOD} = 7.4\ (\pm 0.5) \times 10^{-4}\ min^{-1}$, $k_{OD^-} = 104 \pm 30\ M^{-1}\ min^{-1}$, and p$K_a = 7.92 \pm 0.08$. (B) The rate−pH profile for the DM ribozyme was fit according to the logarithm of eq 6 ($R^2 = 0.98$), and the following parameters were obtained: $k_{max} = 3.13\ (\pm 0.09) \times 10^{-4}\ min^{-1}$ and p$K_a = 6.32 \pm 0.03$. The rate−pD profile for the DM ribozyme was also fit according to the logarithm of eq 6 ($R^2 > 0.99$), and the following parameters were obtained: $k_{max} = 1.57\ (\pm 0.06) \times 10^{-4}\ min^{-1}$ and p$K_a = 6.76 \pm 0.03$. The pL ∼ 5.5, 6.5, 7.5, 8.7, and 9.7 data points in panels A and B were performed in duplicate and on different days, and all data points are shown.

Scheme 4. Double-Subchannel/Single-Protonation/Single-Deprotonation Mechanism

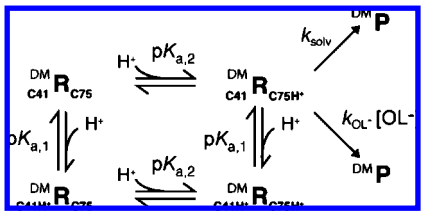

pH plateau of the rate−pH profile and an inverse contribution to the observed solvent isotope effect (see the Results and Discussion).

Two pieces of evidence support specific base catalysis by hydroxide ion rather than general base catalysis by buffer. As discussed by Jencks, if catalysis is specific to hydroxide ion, then the rate will depend only on pH and be independent of the buffer concentration.[46] However, if buffer molecules participate in the reaction, then the rate will increase with buffer concentration, even at constant pH. We found that doubling the concentration of HEPES from 25 to 50 mM at pH 7 in the absence of Mg^{2+} did not affect the reaction rate.[6] Furthermore, Perrotta et al. demonstrated that, in the presence of Mg^{2+}, imidazole only rescues reactions with an inactivating base (U or G) at position 75.[23] This suggests that, when the HDV ribozyme can fold natively, buffer molecules are unable to act as the general base or acid. The bulkiness of HEPES and MES molecules (MW of 238 and 195, respectively) may discourage active participation in the reaction.

When using Scheme 2 to fit the WT rate−pD profiles, we took eq 4 and replaced "H" with "D" to give eq 5:

$$k_{obs,DOD} = \frac{k_{DOD} + k_{OD^-}10^{pD-pK_{DOD}}}{1 + 10^{pD-pK_{R,D}}} \quad (5)$$

where pK_{DOD} is the pK_w of D_2O and p$K_{R,D}$ is the pK_a of the titratable group on the ribozyme in the presence of D_2O. At 1 M ionic strength and 37 °C, the pK_w of D_2O is reported as 14.23.[31]

The rate−pL profiles for the DM ribozyme were fit according to the logarithm of eq 6, which was derived from the single-channel/single-deprotonation mechanism shown in Scheme 3:

$$k_{obs} = \frac{k_{max}}{1 + 10^{pK_{R,L} - pL}} \quad (6)$$

where $pK_{R,L}$ is the pK_a of the titratable group on the ribozyme in the presence of H_2O or D_2O. We note in the Results that a more complex, mechanistically distinct but kinetically equivalent form of eq 6 can be derived from Scheme 4. This has been elaborated upon recently[34] and so was not pursued herein; however, it can be noted that the rate equation describing Scheme 4 has the same high-pH limit as eq 4, as expected from acid−base compensation.

For the proton inventory experiments, the reactions were performed largely as described above. Appropriate volumes of RNA, AS(−30/−7), and buffers in H_2O or D_2O were mixed to obtain the desired mole fraction (n) of D_2O, in which the difference in density of the two solvents was taken into account.[31] Experiments were performed in the plateau regions of pL 6.6 for WT and pL 9.7 for both WT and DM.

Proton inventory data at low pL were fit using the standard Gross−Butler equation. This equation represents the simplest mathematical treatment of proton inventories possible. Derivations of four forms of this equation from simple physical models are provided in Supporting Information, including a more complex population-weighted form developed especially for the system at hand, as well as its simpler non-population-weighted one- and two-proton transfer limits. For the case of two proton transfers, A and B, with nonequivalent transition state fractionation factors (ϕ^T) this equation can be written as[47]

$$k_n/k_0 = (1 - n + n\phi_A^T)(1 - n + n\phi_B^T) \quad (7)$$

where k_0 is the observed reaction rate in H_2O and k_n is the observed reaction rate in a solution with mole fraction of D_2O n. Because of limits in accuracy of data, one often assumes equivalent transition state fractionation factors,[29,31,48] which causes eq 7 to reduce to

$$k_n/k_0 = (1 - n + n\phi^T)^m \quad (8)$$

with $m = 2$ for two proton transfers and $m = 1$ for one proton transfer.

The standard graphical predictions for experimental implementation of eq 8 are as follows. For a one-proton transfer system, a plot of k_n/k_0 versus n will be linear with a slope of $\phi^T - 1$ and an intercept of unity, and for a two-proton transfer system a plot of $(k_n/k_0)^{1/2}$ versus n will be linear with the slope and intercepts given above. A plot of k_n/k_0 versus n for a two-proton system will be concave-up, or "bowl-shaped".

Because the plateau at high pL is due to a compensation of concentrations of the functional forms of an acid and base, proton inventory data at this pL were fit to a population-weighted Gross−Butler equation (eq 9), as well as the standard Gross−Butler equation (eq 8):

$$k_n/k_0 = (1-n)^2 + \phi_{C75}^T n(1-n)10^{\Delta pK_{C75}} + \phi_{OL^-}^E n(1-n)10^{-\Delta pK_{LOL}} + \phi_{C75}^T \phi_{OL^-}^E n^2 10^{\Delta pK_{C75} - \Delta pK_{LOL}} \quad (9)$$

where ribozymes having an acid and a base with HH, DH, HD, and DD compositions are represented by each of the four respective terms in eq 9 and $\phi^E = K_D/K_H$ is termed an "equilibrium fractionation factor" and is defined as a ratio of ground-state fractionation factors and provides a WT inverse equilibrium isotope effect K_H/K_D of 0.43 (see the Discussion for origin). The ΔpK terms are for either ionization of C75 or autoprotolysis of solvent, and each is equal to the value in D_2O minus the value in H_2O. Specifically, ΔpK_{C75} is +0.44 (= 7.92−7.48) (see the Results), whereas ΔpK_{LOL} is +0.85 (= 14.23−13.38). Justification of an equilibrium isotope effect to describe the contribution of OD^- is provided in the Results. Lack of improvement of fits and simulations by more complex versions of this equation is also described in the Supporting Information.

A few assumptions used in arriving at eqs 7−9 are noted. First, we ignored ground-state fractionation factors in eqs 7 and 8, as is typically done for proteins since most functional groups involved in acid−base chemistry appear to have fractionation factors near unity.[49] (An exception is eq 9, involving lyoxide, since its ground-state fractionation factor is significantly less than 1.) Second, we assumed absence of so-called "medium effects", which describe contributions of enzyme protonations at sites other than those involved in the reaction.[49] This is the normal assumption in proteins and seems to hold well in the absence of special circumstances (e.g., participation of RS^-);[49] also, medium effects are often manifested as "dome-shaped" proton inventories, which were not found herein. The influence of solvent on base pairing[30] does not appear to account for the inventories in this study either, as described below.

UV Absorbance-Detected pH Titrations. The RNA oligonucleotide UUCUU was deprotected, desalted, and dissolved in H_2O. In order to test the dependence of the pK_a on ionic strength, titrations were performed in the presence of 0.1, 0.2, 0.33, 0.5, 0.75, 1, 1.2, and 1.5 M NaCl. The concentration of RNA was ∼10 μM, and a total volume of ∼3 mL in a 1 cm path length cell was used. Measurements of UV absorbance were conducted at room temperature using a Beckman Coulter DU 650 spectrophotometer, and pH was monitored using an IQ 150 meter with a PH47-SS ISFET Probe (IQ Scientific Instruments). The meter reading was converted to pH as described below. Titrations were performed similarly to those previously described.[50] At the beginning of each experiment, the spectrophotometer was zeroed on water containing the appropriate concentration of NaCl, and the pH was adjusted to ∼2.5 using 1 M HCl. Then, ∼1 μL of 0.02−0.75 M NaOH was added to the sample, which was followed by mixing, a pH determination, and a UV scan from 220 to 320 nm. To minimize scatter in the data, the cuvette remained in the spectrophotometer for the duration of the experiment, with mixing performed manually with a Pipetman set to 1 mL. Absence of drift in the pH meter was confirmed by occasionally measuring the pH of a 1 mM HCl standard prepared in the ionic strength under examination. Throughout the titration, the change in sample volume was <1%, and so volume corrections were unnecessary.

Plots of absorbance (A) at 240 or 290 nm (which had maximal changes in absorbance) versus pH were fit to eq 10 to obtain the pK_a and Hill coefficient, where A_U and A_P are the absorbance values of the unprotonated and protonated states, respectively, and n_{Hill} is the Hill coefficient reflecting the number of proton binding sites. This equation assumes an all-or-none model if multiple sites are present. An n_{Hill} value near unity is consistent with a one-proton binding site model.

$$A = A_P + (A_U - A_P)\frac{1}{1 + 10^{n_{Hill}(pK_a - pH)}} \quad (10)$$

Inclusion of sloping baselines did not improve the fit or significantly change the pK_a (data not shown) and so were not included in the final pK_a determinations.

(46) Jencks, W. P. *Catalysis in Chemistry and Enzymology*; Dover Publications Inc.: New York, 1969.
(47) Schowen, K. B. Solvent hydrogen isotope effects. In *Transition States of Biochemical Processes*; Gandour, R. D., Schowen, R. L., Eds.; Plenum Press: New York, 1978; pp 225−283.
(48) Smith, M. D.; Collins, R. A. *Proc. Natl. Acad. Sci. U.S.A.* **2007**, *104*, 5818–5823.
(49) Quinn, D. M.; Sutton, L. D. Theoretical basis and mechanistic utility of solvent isotope effects. In *Enzyme Mechanism from Isotope Effects*; Cook, P. F., Ed.; CRC Press, Inc.: Boca Raton, FL, 1991; pp 73−126.
(50) Moody, E. M.; Lecomte, J. T.; Bevilacqua, P. C. *RNA* **2005**, *11*, 157–172.

Determination of pH at Various Ionic Strengths. Perrotta and Been reported that pH meter readings in 4 M LiCl are too low by ~1−2 pH units.[51] We confirmed the presence of low readings on our pH meter and probe (see above for meter and probe specifications) at both low pH (HCl standards) and high pH (NaOH standards) in NaCl solutions that are relevant to the UUCUU titrations and ribozyme reactions. Given these deviations, it was important to convert meter readings into true pH. We first provide corrections for pH during UUCUU titrations and then provide corrections for pH of ribozyme reactions.

1. pH Corrections for UUCUU Titrations. For UUCUU titrations, which were conducted between pH ~ 2.5 and 6.5, we opted to calibrate our meter just on customized HCl standards. We used a two-step process to allow a meter reading to be converted into pH at a given ionic strength. One step involves converting a meter reading into a known concentration of H^+, c_{H^+}, while the other step involves conversion of c_{H^+} into hydrogen ion activity of H^+, a_{H^+}, which affords pH. We describe the calculation of a_{H^+} first, then a process to go directly from the meter reading to pH.

Step 1: Conversion of c_{H^+} into a_{H^+}. The pH of a solution is defined as[50,52,53]

$$\mathrm{pH} = -\log a_{\mathrm{H}^+} \tag{11}$$

The relationship between a_{H^+} and c_{H^+}, is given by

$$a_{\mathrm{H}^+} = c_{\mathrm{H}^+} f_{\mathrm{H}^+} \tag{12}$$

and the activity coefficient, f_{H^+}, can be estimated by an approximate form of the Debye−Hückel equation (at 25 °C), where I is ionic strength of the solution:[52]

$$-\log f_{\mathrm{H}^+} = \frac{0.51\sqrt{I}}{1+\sqrt{I}} - 0.1I \tag{13}$$

According to eqs 11−13, pH at a given ionic strength can be calculated from a known c_{H^+} and ionic strength by the following relationship:

$$\mathrm{pH} = -\log c_{\mathrm{H}^+} - \log f_{\mathrm{H}^+} \tag{14}$$

Step 2:Conversion of a meter reading into pH. To convert a meter reading to a true pH, we constructed calibration curves at each ionic strength using five low-pH standards. Data points on the calibration curve were of known c_{H^+}, made from the following five HCl standard solutions, 10^{-4}, 3.16×10^{-4}, 10^{-3}, 3.16×10^{-3}, 10^{-2} M, each in a fixed background concentration of NaCl. These standards are similar to those described by Perrotta and Been.[51] We then recorded a meter reading in each solution, allowing adequate time for the reading to stabilize. A calibration curve was then constructed by plotting pH versus meter reading for the five HCl standards, where pH was calculated from eq 14. These curves were well described by a straight line ($R^2 = 0.99$) and slopes of 1.07 to 0.98 and intercepts of −0.03 to 0.47, both of which varied monotonically with ionic strength as written. The calibration curves were then used to convert meter readings into pH values for the UUCUU titrations at a given ionic strength. As an example of a calibration curve data point, a 0.01 M HCl/1 M NaCl solution has a theoretical pH of 2.16 (from eqs 13 and 14), but a meter reading of just 1.73.

2. pH Corrections for Ribozyme Reactions. For ribozyme reactions, which were conducted at 1 M ionic strength over a large pH range (pH ~ 5.5−10), both low and high pH standards were used for corrections. This was done using HCl standards of 10^{-3} and 10^{-2} M and NaOH standards of 10^{-3} and 10^{-2} M, each in 1.2 M NaCl. A calibration curve was constructed at 1.2 M ionic strength, since the pH of the 1× buffer was adjusted under these conditions (see above). (A correction from 1.2 to 1.0 M ionic strength was unnecessary because the Debye−Hückel correction for this change is only 0.008, which is small compared to experimental error.) This calibration curve was described by a straight line with slope 1.05 ± 0.004 and intercept 0.297 ± 0.03.

Background

Previously Published pK_a Values for C41 and C75. Before results for the current study are presented, it is necessary to consider pK_a values for the HDV ribozyme from earlier work, including a recent study in which the mechanisms of the genomic WT and DM were compared.[34] The following comparison provides a context in which to compare the divalent ion-free pK_a values from the present study. The various pK_a values are summarized in Table 1. Comparison of WT and DM ribozymes helped reveal the positioning and thermodynamic linkage of protons and metal ions in the ribozyme. The intrinsic[54] pK_a values for C41 and C75 in the WT and DM ribozymes were determined in both the absence and presence of bound Mg^{2+}.

Under conditions that probe the binding of the catalytic Mg^{2+} ion (channel 3), the binding affinity of Mg^{2+} to WT and DM increased as pH *increases*, consistent with previous observation of negative linkage between H^+ and Mg^{2+} binding at the active site.[6] The intrinsic pK_a values for C75 in both WT and DM were determined to be 5.9 ± 0.1 in the presence of bound Mg^{2+} and 7.25 ± 0.2 in the absence of bound Mg^{2+} (Table 1). As expected, these values are close to the observed pK_a values for WT and DM in 10 and ~1 mM Mg^{2+} of 6.1 and 7.1, respectively;[6,28,29] in addition, both pK_a values shift higher by 0.3−0.4 units in D_2O.[6,29] Under conditions that probe the binding of the structural Mg^{2+} ion (channel 2), it was found that the binding affinity of Mg^{2+} to WT (but not DM) increased as pH *decreases*, consistent with binding of the structural Mg^{2+} ion being buttressed by the protonated native base quadruple motif. The intrinsic pK_a values for C41 in WT were determined to be 7.1 ± 0.1 in the presence of bound Mg^{2+} and 5.5 ± 0.1 in the absence of bound Mg^{2+}. These results support binding of two distinct divalent metal ions coupling to pK_a values for two distinct cytosines and provide a context in which to understand pK_a values for these cytosines in the absence of divalent ions.

Although the rate−pH profiles for the WT and DM ribozymes in the presence of Mg^{2+} were indistinguishable at the higher pH values of 6−8, the DM exhibited an ~10-fold steeper loss in rate with pH below pH 6.[34] This observation, together with thermal denaturation studies, suggested that C41 of the DM ribozyme can become protonated and misfold the catalytic core. A double-deprotonation kinetic model was invoked to fit the DM kinetic data, which yielded pK_a values of 5.6 and 5.7 at 10 and ~1 mM Mg^{2+}, respectively, which were assignable to C41. The pK_a of C41 in DM was unusual in that it was insensitive to Mg^{2+} concentration (Table 1). Inhibitory effects of low pH on the properties of C41 in the DM in the presence of Mg^{2+} are critical to the evaluation of the data presented herein on WT and DM in the absence of divalent ions.

Lastly, in the *absence* of divalent metal ions (channel 1), the rate−pH profiles for DM and WT were different.[34] Notably,

(51) Perrotta, A. T.; Been, M. D. *Biochemistry* **2006**, *45*, 11357–11365.
(52) Perrin, D. D.; Dempsey, B. *Buffers for pH and Metal Ion Control*; Chapman and Hall: London, 1974; pp 4−23.
(53) Westcott, C. C. *pH Measurements*; Academic Press: New York, 1978; p 172.
(54) The observed pK_a values for C41 and C75 are a function of Mg^{2+}, which led to a model from which a pK_a can be extrapolated for each cytosine in the presence of bound Mg^{2+}, as well as in the absence of bound Mg^{2+}. These four pK_a values are referred to herein as the "intrinsic pK_a's".

the DM retained a pH dependence that could be fit using a single-deprotonation kinetic model. The pK_a for the DM obtained under channel 1 conditions was 6.45 ± 0.1 and was tentatively assigned to C41 (Table 1). In contrast, WT gave a pK_a of 7.25 ± 0.3 under channel 1 conditions. Differences in the divalent ion-free pK_a values for DM and WT, as well as the aforementioned differences in rate−pH profiles, instigated the divalent ion-free KSIE and proton inventory studies conducted herein.

Results

Rate−pH Profiles for WT and DM Ribozymes. We examined rates of WT and DM ribozyme reactions in the absence of divalent metal ions (channel 1 conditions) as a function of pH and pD (Figure 2). Experiments were conducted in the presence of 100 mM Na_2EDTA to ensure the complete sequestration of polyvalent metal ions and in 1 M NaCl to aid RNA folding.[7,19,55] This concentration of EDTA is sufficient to give a plateau in log k_{obs}−[EDTA] plots from pH 5.0 to 8.0 in 1 M NaCl.[7] We note that the HDV ribozyme self-cleavage activity is not saturable with NaCl, at least out to 2 M NaCl;[56] apparently, NaCl aids but does not complete folding of the HDV ribozyme. Indeed, Perrotta and Been did conduct HDV ribozyme studies out to 4 M NaCl and these too were not saturable.[51] Since it is possible that pH affects Na^+ uptake by the ribozymes, conclusions are made on the basis of *comparison* between WT and DM rate−pH dependencies, in which case most folding effects should cancel (see the Discussion), or at a particular pH such as in proton inventory studies.

The dependence of log k_{obs} on pH for WT is complex (Figure 2A). A plateau region occurs at low pH (5.5−7), followed by a log−linear decrease in rate with intermediate pH (7−9) and a plateau region at higher pH (9−10). Under identical experimental conditions, the DM displays a simpler dependence of log k_{obs} on pH (Figure 2B). At low pH (5.5−6.5) there is a log−linear increase in rate with pH, followed by a plateau region at higher pH (6.5−10). The shape of the DM ribozyme profile in the absence of Mg^{2+} (Figure 2B) appears qualitatively similar to that observed for the WT ribozyme in the presence of Mg^{2+} (channel 3);[6] the mechanistic basis for this similarity in shape is likely due to similarity in compensation of general acid loss by Brønsted base gain (see the Discussion). Overall, the dependencies of rate on pH for WT and DM under channel 1 conditions in H_2O are similar to those previously reported, with pK_a values agreeing within 0.2 units and observed rate constants agreeing within a factor of 2.[7,34] The value for k_{OH^-} is almost 30-fold smaller than the previously reported value, mostly because an ionic strength-corrected pK_w was used to calculate it in the present study (see the Materials and Methods).

The simplest kinetic models that describe WT and DM rate−pH profiles in the absence of divalent ions each require just a single pK_a and are provided in Schemes 2 and 3,

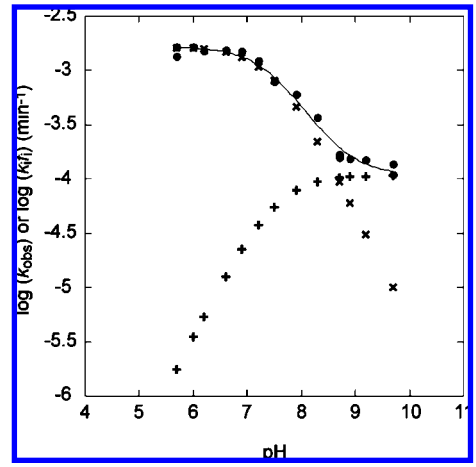

Figure 3. Data and simulations for the WT ribozyme in H_2O. Data (●) are the same as shown in Figure 2A. Kinetic simulations were performed according to Scheme 2. The logarithm of each subchannel rate constant modulated by the fraction of native ribozyme is plotted to see how each subchannel contributes to catalysis. The following kinetic values from Figure 2A were used, which were obtained from fitting the data to eq 4: k_{HOH} = 1.66 × 10^{-3} min^{-1}, k_{OH^-} = 86 M^{-1} min^{-1}, and pK_a = 7.48. Solid line = log k_{obs} (from eq 4), (×) = log($k_{HOH}f_N$) for the solvent-catalyzed subchannel, (+) = log(k_{OH^-}[OH^-]f_N) for the hydroxide-catalyzed subchannel, where f_N = $1/(1 + 10^{pH-pK_{R,H}})$.

respectively. Scheme 2 describes the WT data in which a single-protonation event gives rise to an active ribozyme (RH^+, protonated ribozyme) that can then react via subchannels wherein either solvent or hydroxide acts as the Brønsted base. The hydroxide-catalyzed subchannel is proposed because the rate levels off at the higher pH values, rather than continuing to decrease. Evidence against buffer involvement in the reaction is provided in the Materials and Methods. (Further support for involvement of hydroxide catalysis in this subchannel is provided by a unique inverse equilibrium isotope effect revealed in the proton inventory experiments, discussed below.) The WT data were fit to the logarithm of eq 4, which was derived from Scheme 2, and a pK_a of 7.48 ± 0.07 was obtained (Table 1, Figure 2A). Arguments supporting assignment of this pK_a to C75 are provided below.

To visualize the contribution of the two subchannels to WT catalysis in the absence of divalent ions, kinetic simulations were performed (Figure 3). Simulations were carried out according to Scheme 2 using the kinetic constants provided in Figure 2A. Below pH 7, the solvent-catalyzed subchannel makes the major contribution to the observed rate, whereas above pH 8, the hydroxide-catalyzed subchannel makes the major contribution. Note that according to this model the leveling off at high pH is not due to a second pK_a but rather to a change in the identity of the major subchannel and, therefore, the identity of the active Brønsted base species. Also, leveling off is not indicative of a "kinetic pK_a". Such pK_a's occur because a rate is prevented from going faster than it otherwise would,[57,58] while here it is prevented from going slower than it otherwise would. Overall, the kinetic model in Scheme 2 can account for the WT data.

Scheme 3 is the simplest kinetic model that describes the DM data, in which a single-deprotonation event gives rise to an active ribozyme (R, deprotonated ribozyme) that can then react via just the solvent-catalyzed subchannel.[59] This kinetic

(55) Misra, V. K.; Draper, D. E. *Biopolymers* **1998**, *48*, 113–135.
(56) Plots of log k_{obs} vs log[NaCl] are linear up to the highest concentration of NaCl tested of 2 M: (a) Nakano, S.; Cerrone, A. L.; Bevilacqua, P. C. *Biochemistry* **2003**, *42*, 2982–2994. Values higher than 2 M were not examined because salt concentrations above 1 M begin to denature RNA and DNA in an anion-specific fashion. (See: (b) Bloomfield, V. A.; Crothers, D. M.; Tinoco, I., Jr. *Nucleic Acids: Structures, Properties, and Functions*; University Science Books: Sausalito, CA, 2000; p 308 and references therein. (c) Heerschap, A.; Walters, J. A.; Hilbers, C. W. *Biophys. Chem.* **1985**, *22*, 205–217. (d) Hauser, M.; Bevilacqua, P. C. Unpublished data.) Also, such high concentrations of NaCl could both introduce more trace divalent ions and make them harder to sequester with EDTA.
(57) Fersht, A. *Enzyme Structure and Mechanism*, 2nd ed.; Freeman: New York, 1985; p 475.
(58) Herschlag, D.; Khosla, M. *Biochemistry* **1994**, *33*, 5291–5297.

model is even simpler than the one in Scheme 2, involving one less channel. The DM data were fit to the logarithm of eq 6, which was derived from Scheme 3, and a pK_a of 6.32 ± 0.03 was obtained (Table 1, Figure 2B).[60] Notably, the pK_a observed for DM is more than 1 unit lower than the pK_a observed for WT under identical experimental conditions.

Although Scheme 3 is the simplest kinetic model that fits the DM data, at the molecular level it is not in agreement with the model shown in Scheme 2. In particular, in Scheme 2 the species that reacts to form products is a protonated ribozyme, whereas in Scheme 3 it is a deprotonated ribozyme, which then requires solvent or hydronium ion to act as the Brønsted acid. There is no reason to expect that swapping a structural Watson−Crick base pair ∼15 Å from the active site would reverse the role of C75 in the mechanism from general acid (= GAB model 2) to general base (= GAB model 1) (see Figure 1B for requisite repositioning); indeed, the pK_a's of C75 for WT and DM are identical in the presence of low and high concentrations of Mg^{2+} suggesting that there is not an active site rearrangement (Table 1).[34] Furthermore, there is no reason to expect that hydroxide ion will not contribute to the reaction mechanism of the DM at higher pH values in the same way it does for the WT.

In order to have a mechanism that is globally consistent with WT and DM data, Scheme 4 was developed for DM, which accommodates all of the WT kinetic characteristics, as well as the pK_a for the following C41H$^+$-induced misfolding peculiar to the DM. In this kinetic model, the reactive DM ribozyme species is protonated and can react via solvent- and hydroxide-catalyzed subchannels, as per WT in Scheme 2. To accommodate these common mechanistic features with the rate−pH profile observed in Figure 2B, an additional protonation event must be included. As described in the Background, protonation of C41 in the DM has been shown to induce loss of reactivity;[34] thus, the additional protonation event is likely that of C41. Only a single pK_a is observed in the rate−pH profiles, however (Figure 2B). Arguments in support of assignment of the DM pK_a to C41 are provided below. A more complex, but kinetically equivalent, version of eq 6 can be derived for Scheme 4 (see the Materials and Methods); however, it yields the same pK_a[34] and so was not pursued herein.

Rate−pD Profiles for WT and DM Ribozymes. The WT and DM rate−pD profiles were qualitatively similar to their respective rate−pH profiles (Figure 2) and therefore fit to the logarithm of eqs 5 and 6, respectively.[61] The pK_a values for the WT and DM ribozymes in D_2O are 7.92 ± 0.08 and 6.76 ± 0.03, respectively, 0.44 units higher than their counterpart values in H_2O. D_2O-induced pK_a shifts of this magnitude and direction have also been observed for the ionization of a variety of weak acids, such as an ammonium ion[31] and free cytosine base,[33] as well as the ionization of small ribozymes in the presence of divalent metal ions, including the HDV,[6,25,29] hairpin,[62] and VS[48] ribozymes (all ΔpK_a's = +0.4−0.7). Observations that the rate−pD profiles are similar to the rate−pH profiles and that the pK_a shifts are as expected for ionization of a cytosine are consistent with the metal-free mechanism in D_2O being the same as in H_2O, as expected, and suggest that the observed pK_a values in H_2O and D_2O may belong to cytosine residues, as indicated by kinetic and Raman crystallographic studies.[6,23,28]

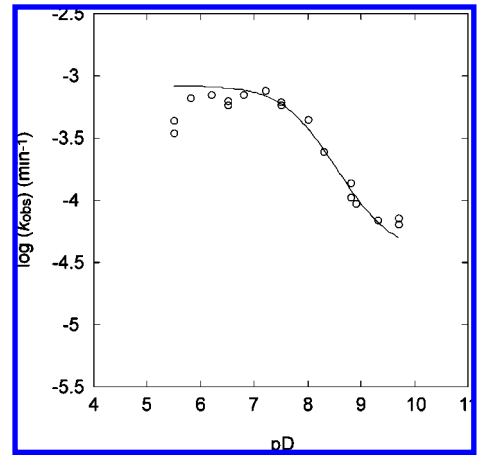

Figure 4. Data and simulations for WT ribozyme in D_2O. Data (○) are the same as shown in Figure 2A. Kinetic simulations were performed according to Scheme 2 beginning with parameters from Figure 2A fits in H_2O. To represent the ∼2-fold KSIE at low pH, k_{HOH} was divided by 2; to represent the pK_a shift, +0.4 unit was added to the pK_a; and to represent the absence of an intrinsic isotope effect at higher pH, $k_{OD^-} = k_{OH^-}$ (Figure 2A). The absence of an intrinsic isotope effect at higher pH is due to canceling of normal and inverse fractionation factors (see the Results and Discussion). Solid line = log k_{obs} from eq 5 using these parameters.

The rate−pH and rate−pD profiles for WT and DM reveal that the reactions in D_2O are ∼2.2−1.9-fold slower in the plateau regions, respectively. These KSIEs are similar in magnitude to KSIEs in the presence of Mg^{2+} for the HDV[6,25,29] and other small ribozymes,[48,62] consistent with proton transfer being rate-limiting. The possibility that these KSIEs arise from a conformational change[30] or a viscosity effect[48] rather than a bond cleavage event is deemed unlikely, as presented below.

Simulation of the effects of D_2O on k_{obs} was performed for WT according to Scheme 2 (Figure 4). The rate−pD profile was largely recapitulated by adjusting the rate−pH profile for a low-pH KSIE of 2 (i.e., k_{HOH} was divided by 2) and a pK_a shift of +0.4 in D_2O (Table 1). No intrinsic isotope effect was used for the higher pH data (i.e., k_{OD^-} was set equal to k_{OH^-}) due to a canceling of normal and inverse rate contributions in 100% D_2O; i.e., a population effect alone accounts for observed rate differences in pure H_2O and D_2O at higher pH (see below). As shown in Figure 4, using these parameters in eq 5 provides a simulated curve that is in good agreement with the data, which is consistent with the kinetic model in Scheme 2.

Proton Inventories at Low pL. To characterize the HDV ribozyme reaction mechanism further, we performed proton inventory experiments in 1 M NaCl/100 mM Na_2EDTA, which report on the number of protons transferred in the rate-limiting step of the reaction. The proton inventory technique involves

(59) The solvent channel is invoked because a hydroxide channel would be expected to a show an increase in rate with higher pH if reacting with a deprotonated C75.

(60) As noted in the text, the pK_a's and rate constants obtained from the WT and DM ribozyme rate−pH profiles in the absence of divalent ions are similar to those previously reported. It should be noted, however, that the previously reported WT ribozyme rate−pH profile was better fit using a double-channel/double-deprotonation kinetic model which gave a second (lower) pK_a. Absence of this lower pK_a in the data presented herein appears to be due to just the lowest pH (pH ∼ 5) data point having a slower rate in those studies. Such a second (lower) pK_a might be present in the WT ribozyme rate−pD profile presented herein (Figure 2A). In our treatment of the data, we fit both WT ribozyme profiles using the simple kinetic model in Scheme 2 but exclude the lowest pD value.

(61) When using Scheme 2 to fit the rate−pD profiles, we took into account that the ionization constant for D_2O is ∼7-fold lower than that for H_2O (see the Materials and Methods).

(62) Pinard, R.; Hampel, K. J.; Heckman, J. E.; Lambert, D.; Chan, P. A.; Major, F.; Burke, J. M. *EMBO J.* **2001**, *20*, 6434–6442.

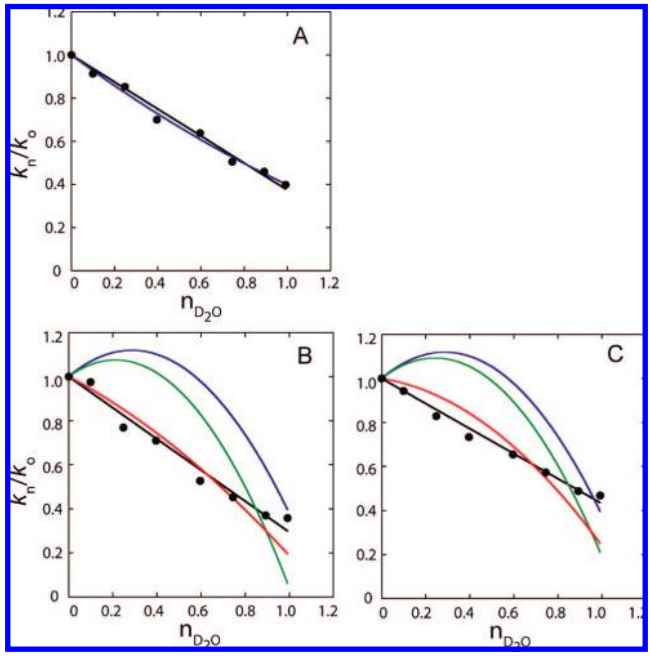

Figure 5. Proton inventories in the three rate−pL plateau regions: WT ribozyme at pL values of (A) 6.6 and (B) 9.7 and (C) DM ribozyme at pL 9.7. All reactions were performed in duplicate and on different days. Average data points are shown. Error bars have been omitted for clarity. The precision for each data point at pL 6.6 was ∼4% (except for the data point at $n \sim 1$, which had a precision of 1.4%). The precision for each data point at pL 9.7 data was less than or equal to 3% for both the WT and DM ribozymes. The *y*-axis is the ratio of the observed rate constant in an H_2O/D_2O mixture (k_n) to that in 100% H_2O (k_0), and the *x*-axis is the mole fraction (n) of D_2O in the mixture. The data in panel A were fit to the Gross−Butler equation (eq 8) for one ($m = 1$) and two ($m = 2$) proton transfers, black and blue lines, respectively. In the case of two proton transfers, equivalent transition state fractionation factors (ϕ^T) were assumed for each transfer. The ϕ^T values are 0.37 ± 0.016 for the one-proton model (black fit; $R^2 = 0.985$) and 0.63 ± 0.009 for the two-proton model (blue fit; $R^2 = 0.991$); these two models cannot be distinguished. The data in panels B and C were fit to a population-weighted Gross−Butler equation (eq 9) that assumes two proton transfers: one from the 2′-OH of U-1 to OL^- in a rapid pre-equilibrium, with equilibrium isotope effect ($1/\phi^E$), and the other in the rate-limiting step from $C75L^+$ to the 5′-O of G1, with transition state fractionation factor (ϕ^T). Solving this equation accurately required that one of the two ϕ values be fixed. Because the one- and two-proton models in panel A could not be distinguished, we fixed ϕ^T to 0.37 according to parsimony and solved for ϕ^E. The ϕ^E values were inverse. For WT at pL 9.7 (panel B), $\phi^E = 2.1 \pm 0.2$ (black fit; $R^2 = 0.975$), whereas for DM at pL 9.7 (panel C), $\phi^E = 3.1 \pm 0.1$ (black fit; $R^2 = 0.987$). Fits to other limiting models were also attempted (see the Supporting Information), including no isotope effect (eq 9 with $\phi^T = \phi^E = 1$; blue "dome-shaped" fit; $R^2 = 0.44$ (WT), 0.46 (DM)); an isotope effect for OL^- only (eq 9 with $\phi^T = 1$; green "dome-shaped" fit; $R^2 = 0.14$ (WT), 0.17 (DM)); and an isotope effect for $C75L^+$ only (eq 9 with $\phi^E = 1$; red fit; $R^2 = 0.906$ (WT), 0.71 (DM)). None of these simpler limiting models fit the data as well.

measuring reaction rate constants in different mixtures of H_2O and D_2O.[31,63] Rate constants are normalized with respect to the rate constant in pure H_2O, plotted versus mole fraction (n) of D_2O, and fit to equations derived from various reaction models. Proton inventories were conducted in the three rate−pL plateaus observed for WT and DM (Figure 2):[64] the low- (Figure 5A) and high-pL (Figure 5B) plateaus of WT and the high-pL plateau of DM (Figure 5C). In this section, we consider the low pL inventory for WT (pL 6.6).

Proton inventories are generally conducted in the plateau regions of rate−pL profiles because it is assumed that under these conditions the concentrations of the functional forms of the acid and base will be constant during the inventory.[65] We begin by asking whether this assumption is justified. According to Scheme 2, which describes the rate−pL profile for WT, the general acid and base in the reaction at low pH, $C75L^+$ and water, respectively, are in their fully functional forms at low pH. The major reaction subchannel for Scheme 2 under these conditions involves k_{solv} and protonated ribozyme. Since the observed pK_a values for WT are 7.48 and 7.92 in H_2O and D_2O, respectively (Table 1), the ribozyme should be nearly fully protonated throughout the pL 6.6 inventory. Also, the concentration of water is largely independent of pH and D_2O composition.[47] Thus, the general acid and Brønsted base should be fully populated throughout the inventory, making it possible to fit the data directly to the standard Gross−Butler equation (eq 8).

The proton inventory for WT at pL 6.6 along with fits to eq 8 are shown in Figure 5A.[66] These proton inventory data decrease in a monotonic and largely linear fashion. The ϕ^T values for WT are 0.37 ± 0.02 and 0.63 ± 0.01 for the one- and two-proton models, respectively, assuming equivalent fractionation factors for each transfer in the latter case as per eq 8. These values are within the range expected for proton transfers involving oxygen or nitrogen atoms,[63] consistent with a cytosine residue(s) being involved in proton transfer. According to eq 8 at the limit of $n = 1$ (i.e., 100% D_2O), the inverse of ϕ^T for one proton transfer, and of $(\phi^T)^2$ for two proton transfers, should give back the KSIE.[31] For the WT fractionation factors, KSIEs of 2.5−2.7 are returned, in agreement with KSIEs from the low-pH plateau in Figure 2A. We also note that a model with three, four, or five equivalent proton transfers would give ϕ^T values of ∼0.74, 0.80, and 0.83, respectively, all of which are larger than expected for proton transfer with oxygen and nitrogen, making such mechanistic scenarios less favorable.

For a KSIE of just 2, discriminating between one and two proton transfers requires a precision of at least 2.8%.[47] The WT ribozyme data at pL 6.6 do not meet this requirement; nonetheless, we can still conclude that at least one proton is transferred in the rate-limiting step. This issue of fitting can be visualized graphically in Figure 5A, in which the straight line (black) for one proton transfer and the "bowl-shaped" line (blue) for two proton transfers fit the data equally well within error (R^2 values of 0.985 and 0.991, respectively). Recent analysis of VS ribozyme proton inventories led to a similar conclusion that at least one proton is transferred in the rate-limiting step.[48] Plots of the square root of the data in Figure 5A, often conducted for proton inventories (see the Materials and Methods),[29,47,62,67] fit well to a straight line (data not shown) but were not compelling enough to distinguish between one- and two-proton inventories. Nonetheless, fitting is valuable in that the values of fractionation factors rule out mechanisms with three or more proton transfers and good fits to the Gross−Butler equation

(63) Venkatasubban, K. S.; Schowen, R. L. *Crit. Rev. Biol.* **1984**, *17*, 1–44.
(64) As discussed later in the text, it is important to perform proton inventories in the plateau regions of the rate−pL profiles; thus, an inventory was not carried out at pL 6.6 for the DM.
(65) Sawata, S.; Komiyama, M.; Taira, K. *J. Am. Chem. Soc.* **1995**, *117*, 2357–2358.
(66) In the case of two proton transfers, the form of the Gross−Butler equation commonly used assumes equivalent transition state fractionation factors (ϕ^T) for the two transfers since, in the absence of additional data, separate fractionation factors are not justified statistically.
(67) Anslyn, E.; Breslow, R. *J. Am. Chem. Soc.* **1989**, *111*, 8931–8932.

suggest that conformational changes are not responsible for the KSIE (see the Discussion).

Proton Inventories at High pL. Next, we consider proton inventories for WT and DM at the higher pL value of 9.0 (Figure 5, parts B and C). As in the previous section, we begin by considering the populations of the functional forms of the acid and base during the inventory. According to Schemes 2 and 4, which provide the simplest global descriptions of WT and DM, respectively, the acid and base in the reaction at pL 9.7 are $C75L^+$ and lyoxide ion, respectively. The pK_a values for the WT ribozyme have been determined to be 7.48 and 7.92 in H_2O and D_2O, respectively (Table 1), which are assignable to C75 (see below and the Discussion); we presume that the pK_a values for C75 are similar in the DM, as its observed pK_a values of 6.32 and 6.76 (Figure 2B) are assignable to C41 protonation and misfolding (see below).[68] In addition, the pK_w values for H_2O and D_2O have been reported as 13.38 and 14.23, respectively, in 1 M ionic strength at 37 °C.[31] Thus, the populations of both the Brønsted acid ($C75L^+$) and base (OL^-) in the reaction are very small at pL 9.7. In addition, over the course of the proton inventory, the amount of $C75L^+$ is favored, whereas the amount of OL^- is disfavored (to an even greater extent). Indeed, these two effects account for the observation in Figure 2A that between pL $\sim$ 7 and 8 the rate−pL profile for the WT in D_2O "catches up" to that in H_2O (i.e., there is more $C75D^+$ than $C75H^+$ in this solvent-catalyzed pH range), only to "fall behind" again above pL $\sim$ 8 (i.e., there is more OH^- than OD^- in this hydroxide-catalyzed pH range) (Figure 2A).

Four models are considered for the high pL proton inventory data, each of which takes into consideration the aforementioned $C75L^+$ and OL^- population changes that occur throughout the inventory. Model 1 is based on the population effects alone (i.e., no ground-state or transition-state fractionation factors are invoked); models 2 and 3 invoke one fractionation factor (i.e., one isotope effect) each; whereas model 4 invokes two fractionation factors, one in the transition state and one in the ground state. We move from model 1 to 4, and then back to models 2 and 3. Ultimately, model 4 is required to explain the data.

Because the populations of the acid and base change throughout the proton inventory, we begin with the simplest possible model, model 1, wherein population changes alone (i.e., in the absence of any KSIEs) attempt to account for the shapes of the WT and DM proton inventories at pL 9.7, which decrease in a monotonic and largely linear fashion (Figure 5, parts B and C) At first, this possibility is appealing because the high-pL population effect in going from 100% H_2O to 100% D_2O is 2.6 ($= 10^{\Delta pK_{LOL}-\Delta pK_{C75}} = 10^{0.85-0.44}$, from high-pL limits of eqs 4 and 5), which is similar to the observed KSIEs for WT and DM at high pL (Figure 2A and Figure 5, parts B and C). However, the following model-driven consideration of rates in *mixed* H_2O/D_2O solvents (i.e., not just pure H_2O or pure D_2O) suggests that this agreement is a coincidence.

We derived a population-weighted Gross−Butler equation (eq 9) (see the Supporting Information) and used it to first attempt to simulate the *full* proton inventory for model 1 (i.e., in the absence of KSIEs where $\phi^T = \phi^E = 1$) (Figure 5B, blue). This equation describes the high pL (i.e., OL^--containing) subchannel depicted for WT and DM in Schemes 2 and 4, respectively, and depicted in Figure 1B (GAB model 2) in which it is now lyoxide rather than water deprotonating the 2′-OL of U-1, although it remains possible that the reaction occurs in more than the one step depicted in Figure 1B (see the Discussion). As expected from the above consideration, good agreement was found between predicted and measured rates in pure H_2O and D_2O. However, in *mixed* isotopic compositions, the measured rate is much slower than that predicted from this simplest possible model of population changes alone. In fact, the rate predicted near $n = 0.4$ is greater than that in 100% H_2O, predicting a so-called "dome-shaped" reaction plot (these poor fits are shown in Figure 5, parts B and C, for illustrative purposes). This prediction is obverse to the observed decrease in rate at $n = 0.4$, and thus we can rule out the simplest model of population effects only. Nonetheless, the populations of $C75L^+$ and OL^- *do* change throughout the inventory, going up and down, respectively, as the fraction of D_2O increases, and the remaining three reaction models must take these population changes into account.

Simulations (not shown) reveal that the predicted dome arises because the $C75D^+/OH^-$ population cross-term of eq 9 (term 2) is especially favored in mixed solvents, as described above. Only by damping this term with a transition state fractionation factor less than 1 (i.e., a normal KSIE) can the observed inventory curve be restored. Since the deuterium in this cross-term is on C75, this predicts that $C75L^+$ will contribute to the isotope effect in a normal manner, which is consistent with the Mg^{2+}-free proton inventory at pL 6.6 (Figure 5A) as well as previous inventories in the presence of Mg^{2+}.[25,29] This argument holds for DM as well as WT.

For model 4, fixing the fractionation factor for C75 (ϕ^T_{C75}) to 0.37, which was the value obtained for the one-proton inventory on WT at pL 6.6 (Figure 5A), and fitting the data to the population-weighted Gross−Butler equation (eq 9) gives *inverse* equilibrium isotope effects for OL^- for WT and DM with equilibrium fractionation factors, $\phi^E_{OL^-}$ of 2.1 and 3.1, respectively (Figure 5, parts B and C).

In 100% D_2O, the inverse contribution from OL^- essentially cancels the normal contribution from $C75L^+$, as expected since population effects alone appear to account for the 100% D_2O data; i.e., at $n = 1$, only term 4 of eq 9 is nonzero and in this term the product of the normal and inverse fractionation factors ($\phi^T_{C75}\phi^E_{OL^-}$) is near unity and the population contribution of $10^{\Delta pK_{C75}-\Delta pK_{LOL}}$ is similar to the inverse of the KSIE. An inverse contribution for OL^- is consistent with expectations for a rapid pre-equilibrium deprotonation of the 2′-OL by OL^- (see the Discussion); the fractionation factor for OL^- is assigned a superscript of "E" to denote that its isotope effect is an equilibrium, or ground-state, effect.[31,47,69]

Population-weighted models of intermediate complexity (i.e., involving just one fractionation factor rather than two), models 2 and 3, were considered but do not fit the proton inventory data well. For example, a one-proton inventory derived for OL^- but not $C75L^+$ contributing to the isotope effect (model 2) is shown in green and a one-proton inventory derived for $C75L^+$ but not OL^- contributing to the isotope effect (model 3) is shown in red (these poor fits are shown in Figure 5, parts B and C, for illustrative purposes). Neither model accounts for the data. Importantly, swapping the normal and inverse contri-

(68) The claim that the WT and DM ribozymes have the same rate-limiting step is also supported by observation that the rates for the WT and DM in the high-pH plateau are within ~2-fold of one another (Figure 2), suggesting that both ribozymes populate the same channel (see the Discussion).

(69) Gold, V.; Grist, S. *J. Chem. Soc., Perkin Trans. 2* **1972**, 89–95.

butions between $C75L^+$ and OL^- made the fit much worse with a dome-shaped curve that had a maximum of ~2.5 near an *n* of ~0.5 (not shown). More complex models were also considered but provided data similar to that from eq 9 (see the Supporting Information).

In summary, the simplest model that explains the proton inventory data at high pL while taking into account the D_2O-dependent population changes in $C75L^+$ and OL^- has two fractionation factors: a normal kinetic isotope effect on $C75L^+$ with a fractionation factor of ~0.37 and an inverse equilibrium isotope effect on OL^- with a fractionation factor of 2.1−3.1.

Dependence of pK_a Values on Ionic Strength. The rate−pL and proton inventory experiments were conducted in the presence of 1 M NaCl and 100 mM Na_2EDTA to aid RNA folding and ensure complete sequestration of polyvalent ions.[7,19] Although effective in promoting HDV reactivity in the absence of divalent ions, high ionic strength conditions have the potential to perturb other characteristics of the RNA, including pK_a values. Fersht points out that ionization should be less sensitive to ionic strength for a cationic acid (HA^+ to $H^+ + A$) than a neutral acid (HA to $H^+ + A^-$), since there is no change in ionic strength in the former process.[57] Cytosine and cytidine are cationic acids, and literature reports confirm little ionic strength dependence of the pK_a for these species.[70] For both cytosine and cytidine, the pK_a of N3 is essentially invariant upon increasing the ionic strength from 0 to 1 M.[70]

Introduction of nearby charge on the surface of a biopolymer, however, can alter the dependence of a pK_a on ionic strength.[57] We therefore conducted pH titrations on an unstructured oligonucleotide, $UU(CH^+)UU$ (HA^{3-} to $H^+ + A^{4-}$). A pentamer was chosen for study because it flanks the cytosine with four negative charges, which begins to mimic the ionic environment that a non-base-paired cytosine might experience in an unstructured RNA. In addition, uracil was chosen as the nonionizing base because it is a poor stacker,[71,72] allowing the pentamer to remain unstructured throughout the titration. Absorbance data were collected as a function of pH and fit to a two-state binding model using the Henderson−Hasselbalch equation (eq 10).[50] Because ionic strength affects both the activity of H^+ and pH meter readings, a calibration curve was constructed to convert meter readings into pH (see the Materials and Methods).

Plots of absorbance at 240 and 290 nm increased and decreased with pH, respectively, as expected (Figure 6, parts A and B).[50] This ionization event is assignable to the N3 of the C of UUCUU on the basis of these absorbance changes and also because this is the only functional group in UUCUU with a pK_a near 4.[50,73] Plots were well described by eq 10 and gave Hill coefficients near unity, consistent with a single ionization event.

As ionic strength was increased from 0.1 to 1 M, the pK_a decreased by ~0.4 units and leveled off at a value of ~4.25 (Figure 6C), with this pK_a value being similar to those observed for free cytosine, which range from 4.0 to 4.3 in moderate ionic strength.[70] This decrease in the pK_a along with observation that the C of UUCUU has properties similar to isolated cytosine is consistent with nearly complete screening of favorable electrostatic interactions between protonated C and the nearby phosphate backbone by salt at ionic strength near 1 M.

Effects of ionic strength on the pK_a of C in UUCUU can be used to guide expectations for C75 and C41. Calculations of pK_a shifts using solutions to the Poisson−Boltzmann equation provide a separate, semiquantitative guide to pK_a shifting in the HDV ribozyme.[74] These calculations are able to parse contributions to pK_a shifting into base−phosphate and base−base contributions. C75 has the loaded proton free to transfer, and so the origin of its pK_a shift appears to be in electrostatics, whereas C41 has its loaded proton sequestered in hydrogen bonding, and so the origin of its pK_a shift appears to be in favorable hydrogen bonding.[74,75] Indeed, nonlinear Poisson−Boltzmann calculations reveal that the catalytic nucleobase C75 is found in a pocket of high negative electrostatic potential.[7,74] Thus, in the same way that the pK_a of UUCUU decreases with increasing ionic strength, the pK_a of C75 might be expected to decrease with increasing ionic strength.

The structural nucleobase C41, on the other hand, is not found in a region of especially negative electrostatic potential.[7,74] It appears that the driving force for pK_a shifting of C41 in WT is the gain of hydrogen bonding within the base quadruple (Figure 1C).[76] Thus, the pK_a of C41 is not expected to be sensitive to ionic strength, which is consistent with the absence of anticooperative interactions between protonation of C41 and binding of a nearby metal ion.[7,34] The effects of ionic strength on the pK_a's of C75 and C41 will be used to help guide assignment of the observed pK_a values in the Discussion.

Discussion

The five naturally occurring small ribozymes catalyze phosphodiester bond cleavage proficiently in the absence of catalytic divalent metal ions. Nucleobases have been shown to play catalytic roles in the cleavage mechanisms of these ribozymes and to have pK_a values shifted toward neutrality. However, assigning the specific mechanistic roles that the nucleobases play in bond breaking and making remains a challenge. In the case of the HDV ribozyme, C75 has been implicated in proton transfer. Das and Piccirilli provided strong support for C75's mechanistic role *in the presence of* Mg^{2+}, that of general acid in bond cleavage,[24] but its mechanistic role *in the absence of* Mg^{2+} has remained elusive. Mechanistic roles of nucleobases in the absence of divalent ions have general implications for the catalytic ability of other RNA molecules as well as the RNA world hypothesis.

A key observation in deciphering the catalytic role of C75 was inversion of the rate−pH profile upon removal of the catalytic divalent ion, which implicated C75 as the general acid.[6] However, interpretation of this result was complicated by a report that the rate−pH profile is flat for a double mutant that allows the base quadruple to form without protonation of C41, suggesting that the divalent ion-free pK_a observed for WT is for ionization of C41 rather than C75.[19]

(70) Izatt, R. M.; Christensen, J. J.; Rytting, J. H. *Chem. Rev.* **1971**, *71*, 439–481.
(71) Richards, E. G.; Flessel, C. P.; Fresco, J. R. *Biopolymers* **1963**, *1*, 431–446.
(72) Turner, D. H.; Bevilacqua, P. C. Thermodynamic considerations for evolution by RNA. In *The RNA World*; Gesteland, R. F., Atkins, J. F., Eds.; Cold Spring Harbor Laboratory Press: Cold Spring Harbor, NY, 1993; pp 447−464.
(73) Saenger, W. *Principles of Nucleic Acid Structure*; Springer-Verlag: New York, 1984; p 556.
(74) Tang, C. L.; Alexov, E.; Pyle, A. M.; Honig, B. *J. Mol. Biol.* **2007**, *366*, 1475–1496.
(75) Bevilacqua, P. C.; Brown, T. S.; Nakano, S.; Yajima, R. *Biopolymers* **2004**, *73*, 90–109.
(76) Protonation of C41 in the DM also appears to be driven by hydrogen bonding, although in formation of a misfold (see below).

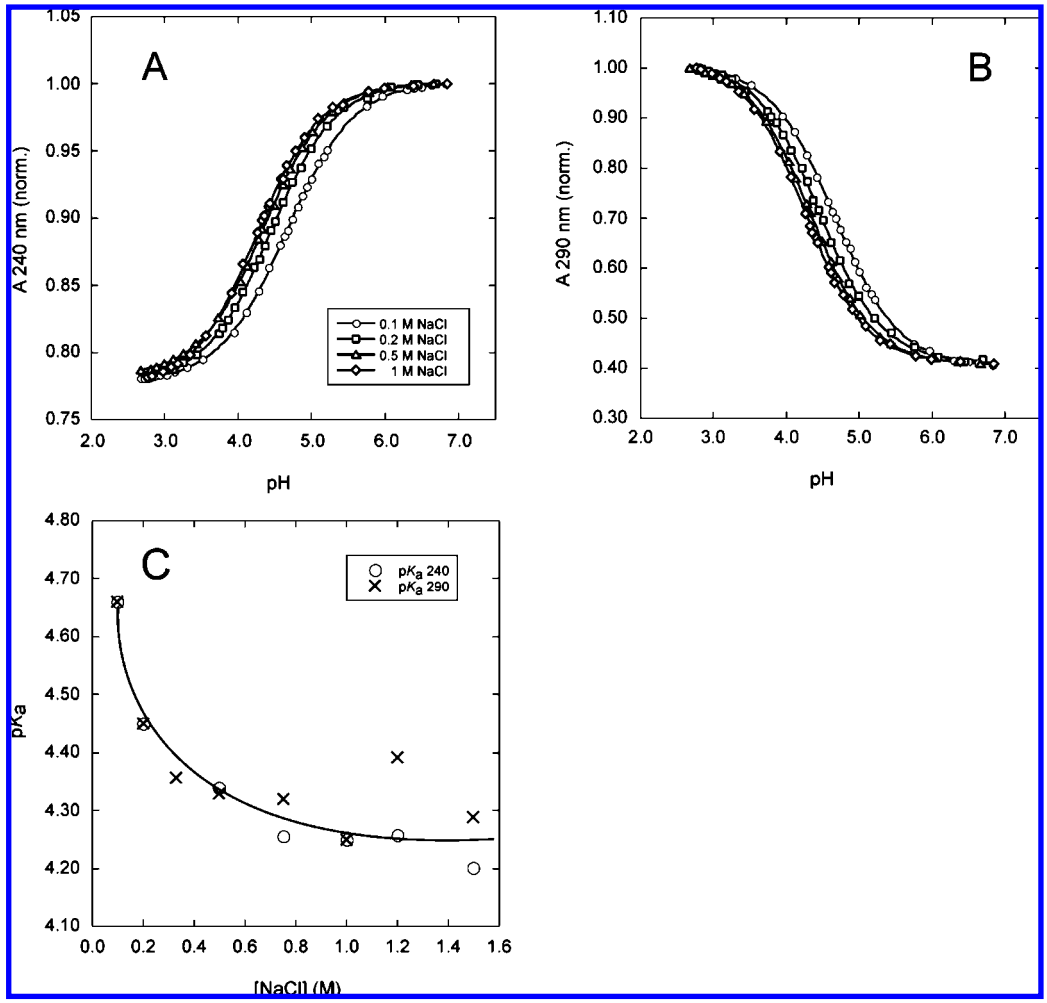

Figure 6. Determination of the pK_a of C in a single-stranded RNA oligonucleotide at various ionic strengths. Representative titrations of UUCUU RNA with NaOH monitored at (A) 240 nm and (B) 290 nm as a function of ionic strength. Each titration curve was fit to eq 10. In all cases, the Hill constant n is approximately 1. (C) Plot of pK_a vs [NaCl]. pK_a values at both 240 (○) and 290 nm (×) are plotted. The pK_a levels off at high concentrations of NaCl near a value of 4.25, which is similar to the value for cytosine in Na^+ concentrations ranging up to 1 M (ref 70). The solid line is a smooth curve that follows the trend.

Proton inventories have provided deep insight into the rate-limiting step and number of proton transfers in protein enzyme and model systems that catalyze the same phosphodiester cleavage reaction as the HDV ribozyme. For example, Matta and Vo found that the second step of RNase A, opening of a 2′,3′ cyclic phosphate, has an inventory of two, consistent with the expected number of transfers in a concerted mechanism.[77] In addition, Anslyn and Breslow found inventories of one or two for phosphodiester-cleaving cyclodextrin models of RNase A synthesized with one or two imidazoles, respectively, in their reaction cavities. These examples suggest that proton inventories have the potential to help understand the mechanism of RNA enzyme-catalyzed phosphodiester bond cleavage reactions as well.[67]

Herein, rate−pL and proton inventories were conducted for WT and DM HDV ribozymes and interpreted using a global kinetic model that accommodates all of the data: rate−pL plateaus, pK_a values, pK_a shifts in D_2O, DM misfolding, normal and inverse isotope effects, and electrostatic dependencies of pK_a values. The data are best accommodated by a model in which the pK_a for the DM belongs to C41, whereas the pK_a for WT belongs to C75. Thus, inversion of the WT rate−pH profile upon removal of the catalytic divalent ion supports a mechanism with C75 as the general acid in bond cleavage both in the presence and absence of divalent ions, with hydroxide ion acting as a specific base at higher pH values. In the Discussion, we consider support for this and alternative kinetic models.

Nature of the Rate-Limiting Step. One possibility is that the observed pK_a's arise from a change in the rate-limiting step from chemistry to a conformational change—a so-called "kinetic pK_a".[57] This effect has been found to occur in the case of the group I ribozyme.[58] Such a scenario would imply that the observed pK_a does not belong to C41 *or* C75. A putative change in rate-limiting step would occur when the profile switches from the pH-dependent to the pH-independent arm.

In a careful mechanistic examination of the origin of KSIEs in ribozymes, Tinsley et al. demonstrated that binding and dissociation of substrate to a trans acting HDV ribozyme gave rise to KSIEs of 2−2.5 and ∼1.5, respectively.[30] Thus, the presence of a KSIE is not enough to be certain that bond cleavage is rate-limiting. These authors then showed that proton inventories for substrate binding do not conform to the Gross−Butler equation, which led them to emphasize the

(77) Matta, M. S.; Vo, D. T. *J. Am. Chem. Soc.* **1986**, *108*, 5316–5318.

importance of carrying out proton inventories in concert with KSIE studies.[30]

Although we used a cis acting ribozyme that does not participate in bimolecular substrate binding and dissociation, conformational changes involving the formation and dissociation of base pairs are still possible. As presented in the Results, the proton inventory conducted on WT at pL 6.6 obeys the Gross−Butler equation (Figure 5A), whereas the KSIEs on WT and DM at pL 9.7 conform to a population-weighted Gross−Butler equation (Figures 5, parts B and C), as well as the standard Gross−Butler equation (not shown in Figure 5, parts B and C). It is therefore unlikely that the WT and DM KSIEs observed herein arise from conformational changes.

Given that WT and DM ribozyme reactions proceed ~3000-fold slower in the absence of Mg^{2+} than in the presence of 10 mM Mg^{2+}, it might seem surprising that the reaction could be limited by a chemical change. However, similar observations have been previously reported for HDV and VS ribozyme reactions. In the case of the HDV ribozyme, the C75A mutant in Mg^{2+} proceeds ~300- and 4000-fold slower than WT in genomic[6] and antigenomic[23] contexts, respectively, yet still gives the expected pK_a in rate−pH profiles. Similarly, the A756C mutant of the VS ribozyme self-cleaves ~700-fold slower than wild-type VS ribozyme, yet shows similar pK_a and KSIE values.[48] In the slow-reacting HDV and VS ribozymes, it has been suggested that an inactive fold of the ribozyme is in rapid equilibrium with a catalytically competent one such that changes in the rate of the cleavage step are still sensed.[7,48,78] Perhaps rapid equilibrium occurs because these ribozymes have difficulty specifying the native fold.

Evidence Against Viscosity Effects. The viscosity of D_2O is ~1.2-fold higher than that of H_2O;[47] it is therefore important to know whether an observed KSIE is simply the effect of the more viscous D_2O slowing a diffusion-limited reaction.[48,79] The observation in Figure 2A that rates in D_2O and H_2O are nearly identical between pL 7 and 8, only to be different at lower and higher pL values, makes this possibility unlikely because it requires the remote scenario that viscosity is only a factor at intermediate pL values. That the KSIEs are not due to viscosity effects suggests that the rate-limiting step is not a diffusion process, which is consistent with the conclusions from the previous section that the rate of the ribozyme reaction is not limited by a conformational change.

pK_a Assignments in the DM. Next, we consider the molecular origin of the observed pK_a for the DM ribozyme rate−pH profile, as well as the mechanistic basis for the shape of the profile. The DM ribozyme was designed to form the base quadruple without protonation of C41 (Figure 1D). Although this mutant should simplify rate−pH profiles, we recently found that in the presence of Mg^{2+} (channel 3) the DM ribozyme loses activity below pH 6 with a second-order dependence on H^+ concentration.[34] The probable cause of this effect is that protonation of C41 induces formation of a misfolded base quadruple that renders the DM ribozyme inactive.

Protonation of C41 could cause misfolding of the DM ribozyme in the absence of Mg^{2+} as well.[80] When pH is higher than ~6, neutral C41 can form the "native" base quadruple. When pH is lowered, cationic C41 can engage in a new interaction, potentially with the Hoogsteen face of the nearby G74 as previously described,[34] or in an altered register involving the O2 and $N3H^+$ of C41 with the Hoogsteen face of A73. Either of these arrangements has the potential to inactivate the ribozyme due to alteration of the surrounding hydrogen-bonding network.

The pK_a associated with such adjustments of hydrogen-bonding interactions is not expected to be sensitive to ionic strength. This is especially true for C41 since the electrostatic potential of the ribozyme is not especially negative near C41.[7,74] As presented in the Results, the observed pK_a for C41 in the DM is not especially sensitive to ionic strength. Its value is 5.7, 5.6, and 6.32−6.45 in 0.87 mM Mg^{2+}, 10 mM Mg^{2+}, and 1 M NaCl/100 mM Na_2EDTA, respectively (Table 1).[6,34] Moreover these values are outside the error limit on the observed pK_a values of WT (7.25−7.48 in 1 M NaCl/100 mM Na_2EDTA), suggesting that the pK_a measured for the DM is distinct from that measured for WT (see below). Thus, the pK_a for the DM is assigned to C41 rather than C75.

pK_a Assignments in the WT. The WT and DM ribozymes display opposing behavior as pH is lowered from 7 to 5 (Figure 2). While the rate of the DM decreases over this range, the WT rate increases; in other words, the two rate−pH profiles are inverted with respect to one another. This observation suggests that the molecular origins of the two observed pK_a's are different. Increase in the rate of the WT reaction with decreasing pH is consistent with a protonation event facilitating the reaction, whereas decrease in the rate of the DM reaction with decreasing pH is consistent with a protonation event inhibiting the reaction. Given that the protonation event for the WT appears to not be associated with a conformational change, it is most likely due to ionization of C41 or C75.

The observed pK_a for the WT is sensitive to the presence of a catalytic Mg^{2+} ion presumably because protonated C and the catalytic Mg^{2+} ion are close in space. Its value is 7.1, 6.1, and 7.25−7.48 in 0.87 mM Mg^{2+}, 10 mM Mg^{2+}, and 1 M NaCl/100 mM Na_2EDTA, respectively (Table 1).[6,34] These pK_a values support the local environment for C75 in the absence of Mg^{2+} being similar to that in its presence and lack of an influence of ionic strength on pK_a. Indeed, the value of 7.48 ± 0.07, measured herein in 1 M NaCl/100 mM Na_2EDTA, is nearly equal to the intrinsic pK_a value of 7.25 ± 0.2 determined under channel 3 conditions extrapolated to no bound Mg^{2+}.[34] The lack of coupling of this pK_a with ionic strength is consistent with protonated C75 being protected from the influence of bulk monovalent ions; else, its pK_a should be lowered by ionic strength as inferred from pH titrations of UUCUU as a function of ionic strength (Figure 6). A buried C75 in the active site is consistent with the crystal structure of the RNA both in the presence and absence of divalent ions.[15,17,18]

In particular, a recent 2.4 Å cocrystal structure of the C75U-inactivated precleaved HDV ribozyme in the presence of Tl^+ monovalent ions shows a buried active site.[18] It has 15 Tl^+ ions bound to the RNA, but only three of which are positioned in or near the active site. Two of the three active site metal ions interact with the ribozyme in ways that may not reflect catalysis—through the O4 of the U75 mutation or via water

(78) Brown, T. S.; Chadalavada, D. M.; Bevilacqua, P. C. *J. Mol. Biol.* **2004**, *341*, 695–712.

(79) Blacklow, S. C.; Raines, R. T.; Lim, W. A.; Zamore, P. D.; Knowles, J. R. *Biochemistry* **1988**, *27*, 1158–1167.

(80) The diagnostic of DM misfolding in the presence of Mg^{2+} was a slope of 2 in the low-pH arm of the log rate−pH profile. In the absence of Mg^{2+}, this slope is only 1. This can be explained because lowering pH causes two unfavorable events in the presence of Mg^{2+}, depopulation of magnesium hydroxide and protonation of C41, but only one unfavorable event in the absence of Mg^{2+}, protonation of C41, since solvent is the apparent Brønsted base.

bridging to the active site. However, the third ion forms inner-sphere interactions with the 2′-OH of U-1, a nonbridging oxygen of the scissile phosphate, and the N7 of G1 (Figure 1B).[18] This observation suggests that a monovalent ion might serve a role in activating the 2′-OH to attack the scissile phosphate, potentially by acting as a Lewis acid to stabilize the 2′-oxyanion and/or neutralize charge development at the scissile phosphate.[18] Ammonium ions, it seems, catalyze the cleavage reaction in a unique fashion, as typified by a large *inverse* thio effect,[51] a result that does not preclude a functional role for an alkali metal. Moreover, a monovalent ion would be expected to have less influence on the pK_a of C75 than a bound divalent ion, consistent with a higher pK_a in 1 M NaCl (Table 1).

Proton Inventories at Low pH: The Case for a One-Proton Inventory. Shih and Been reported a one-proton inventory for the antigenomic HDV ribozyme in the presence of 10 mM Mg^{2+},[25] whereas we reported a two-proton inventory for the genomic HDV ribozyme in the presence of Mg^{2+}, albeit with a bowl shape that was "shallower" at higher (10 mM) than lower (0.87 mM) Mg^{2+}.[29] One possibility is that the number of protons transferred depends on the reaction conditions, a conclusion strengthened by the fact that the latter data were collected in the same laboratory with the same RNA constructs as the present study.

In the presence of high concentrations of a Brønsted base, such as hydrated magnesium hydroxide ion (channel 3 of Scheme 1) or water (channels 1 and 2 of Scheme 1 at lower pH), the sole transfer of the proton to the leaving group may become rate-limiting. This may also be the case for channels 1 and 2 of Scheme 1 at higher pH, in which hydroxide ion could remove the 2′-OH in a rapid equilibrium prior to leaving group protonation (see below). Changing of the proton inventory from one to two has been directly demonstrated for a cyclodextrin mimic of RNase A in which the numbers of protons transferred in the transition state depended on the number of imidazole groups attached near the top of the cyclodextrin.[67] Also, an RNase A mimic with a single imidazole has been implicated in a mechanism involving general acid catalysis (by the imidazole) without general base catalysis; moreover, this mimic displays a nearly identical rate−pH profile as WT.[81] These considerations support participation of just one proton transfer rather than two in the HDV ribozyme in the absence of Mg^{2+} at low pL.

Origin of the Inverse Contribution of Hydroxide Ion to the Observed KSIE. If the pK_a observed for WT is assignable to C75 and if inversion of the rate profiles upon catalytic divalent ion removal implicates C75 as the general acid, then the plateau in the high-pH region of the rate−pH profile (Figure 2A) must arise from involvement of hydroxide ion as a Brønsted base. The following discussion provides further support for involvement of hydroxide ion in the reaction at high pH by considering the molecular basis for the inverse contribution to the KSIE observed at high pL (Figure 5, parts B and C).

Previous studies have shown that OD^- in D_2O is less stable than OH^- in H_2O.[31,69] This property has the potential to make OD^- more likely than OH^- to deprotonate a 2′-OL and form a 2′-alkoxide on U-1; however, this argument holds only under certain conditions. The primary argument for why OD^- is less stable than OH^- is that the lyoxide ion uses its lone pairs to form three strong hydrogen bonds with L_2O and these are weaker for OD^- in D_2O. However, if there are similar hydrogen bonds in the next state on the reaction coordinate, then the effect of weaker hydrogen bonding in the reactant state will be canceled and no significant isotope effect will be observed.[31,63,69] Transition states involving OL^- generally have similar hydrogen bonding as the reactant state, in so-called transition state "solvation catalytic proton bridges", and so suffer approximately the same stability loss in D_2O as the lyoxide ion.[49,63] Thus, involvement of hydroxide ion is expected to have little effect on an intrinsic KSIE.

Likewise, if an equilibrium process results in the formation of three strong hydrogen bonds from solvent molecules to the 2′-alkoxide of U-1, any isotope effects should approximately cancel. However, the crystal structure of the HDV ribozyme in Tl^+ ions reveals that the 2′-OH of U-1 is directly coordinated to a monovalent ion.[18] This interaction should liberate one or more of the solvating waters and lower the pK_a of the 2′-alkoxide, which would in turn weaken interactions with any remaining waters.[82]

The aggregate ground-state fractionation factor for lyoxide is 0.43, determined from release of the three waters each with a fractionation factor of 0.7 coupled with strengthening of the internal stretching of the $O-L^-$ bond with a fractionation factor of 1.25, ($0.43 = 0.7^3 \times 1.25$).[31] Because of the aggregate fractionation factor, an inverse contribution to k_{obs} of 2.3 (= 1/0.43) is expected for lyoxide ion acting in an inverse *equilibrium* isotope effect (i.e., $\phi^E = K_D/K_H = 2.3$).[69] Inverse equilibrium isotope effects of 2.1 and 3.1 determined for WT and DM, respectively (Figure 5, parts B and C) are in good agreement with the expected ϕ^E of 2.3.

This analysis leads us to conclude that the inverse contribution to the isotope effect occurs because of a rapid pre-equilibrium in which the potent lyoxide ion deprotonates the 2′-OH; this then attacks the neighboring phosphorus to afford a trigonal bipyramidal intermediate. This high-energy 2′-oxyanion intermediate is resolved in a rate-limiting step involving protonation of the 5′-bridging oxygen by protonated C75 with a normal isotope effect. Such a nonconcerted, stepwise reaction agrees with experiments on cleavage of dinucleotides by imidazole in solution[75,83,84] and is consistent with recent DFT and QM−MM calculations on the HDV ribozyme, which favor a two-step reaction, the last step of which is protonation of a trigonal-bipyramidal phosphorane at the 5′-bridging oxygen.[41,42] It has been suggested that the exocyclic amine of N3-protonated C75 may protonate a nonbridging oxygen of the scissile phosphate to afford the phosphorane, analogous to possible involvement of the N6 of N1-protonated A38 in the hairpin ribozyme.[41,75] In these cases, deprotonation of the amino group of cationic A or C would afford a neutral imino tautomer. This mechanism is consistent with observation that C75A is reactive in the HDV ribozyme but C75U, which lacks an exocyclic amine, is not.[6,23]

Where are the "Missing" pK_a's? If the observed pK_a for the DM is assignable to C41, then where is its pK_a for C75? Likewise, if the observed pK_a for WT is assignable to C75, then where is its pK_a for C41? We begin by considering the DM.

As mentioned, the rate−pH profile for DM in the absence of Mg^{2+} (Figure 2B) appears qualitatively similar to that for WT in the presence of Mg^{2+} (channel 3).[6] This similarity can be accounted for by Brønsted acid−base compensations (Scheme

(81) Orth, E. S.; Brandao, T. A.; Milagre, H. M.; Eberlin, M. N.; Nome, F. *J. Am. Chem. Soc.* **2008**, *130*, 2436–2437.

(82) Unfortunately, specific waters could not be resolved in this portion of the structure.

(83) Anslyn, E.; Breslow, R. *J. Am. Chem. Soc.* **1989**, *111*, 4473–4482.

(84) Breslow, R.; Chapman, W. H. J. *Proc. Natl. Acad. Sci. U.S.A.* **1996**, *93*, 10018–10021.

4). The WT ribozyme under channel 3 conditions has a plateau over the higher pH range most readily explained because the decrease in the concentration of the putative general acid, protonated C75, with pH is *compensated* for by the increase in concentration of the putative general base, hydrated magnesium hydroxide ion, with pH. Likewise, for DM under channel 1 conditions the plateau regime over the higher pH range appears to occur because the decrease in the concentration of the putative general acid with pH, protonated C75, is *compensated* for by the increase in concentration of the hydroxide specific base with pH. The proton inventory data at high pH could be accounted for using a two-proton inventory population-weighted Gross−Butler equation with an inverse contribution from hydroxide ion (Figure 5, parts B and C), consistent with the involvement of hydroxide ion in the reaction.

Since the shapes of the WT and DM rate−profiles are different, it is not immediately clear that the two ribozymes share a common rate-limiting step at high pH. However, Schemes 2 and 4, which explain the WT and DM data respectively, have identical lyoxide subchannels, allowing for this possibility. It is noteworthy that the rate−pH profiles for WT and DM level off at approximately the same k_{obs} value in both H_2O and D_2O, albeit with a slight rate enhancement by the DM at higher pH (see Figure 2, parts A and B, which share the same *y*-axis). A similar effect was observed by Wadkins et al., in which the DM leveled off with a slightly greater k_{obs} than WT at pH 8.5, the highest pH value they tested.[19] Similarities of rates, proton inventories, and observed KSIEs for WT and DM at pL 9.7 suggest that the two ribozymes share a common mechanism under these conditions involving C75. It is possible that protonation of C41, which occurs near the pK_a for C75, cancels the gain in rate as pH is lowered from ~8 to 6, as seen in WT, leaving only the inactivation by C41 at pH 6 and lower.[80]

Next, we consider the absence of an observed pK_a for C41 in the WT. First, we note that the pK_a for C41 is not observable under "standard" channel 3 conditions in the presence of millimolar concentrations of Mg^{2+} either.[6] In this case, absence of an observable pK_a was attributed to exceptionally stable folding of the ribozyme. One possibility is that while protonation of C41 in DM can lead to a hydrogen-bonding shift to the "right" in the standard drawing of the quadruple (Figure 1, parts C and D), deprotonation of C41 in the WT can lead to a hydrogen-bonding shift to the "left". These opposing movements may be enough to inactivate and retain activation of the ribozyme, respectively. Because C41 deprotonation is functionally silent, it is not depicted in Scheme 2, which is for WT.

Absence of a functional consequence of C41 ionization in WT is consistent with NAIM experiments that concluded that only C75 ionization is functionally important.[26] It is also consistent with the findings of a recent Raman study on crystals of the genomic HDV ribozyme, in which ionization of C41 was spectroscopically silent, presumably because C41 simply underwent a base-pairing shift, which would not have been detected in the single-stranded portion of the Raman spectrum.[28]

Lastly, we carried out structure mapping experiments on both WT and DM at pH 5 and 7 in the presence of RNases A and T1. Overall, very little change was found as a function of pH (data not shown), suggesting that there are no large-scale conformational changes associated with ionizations of C41 and C75, although more subtle rearrangements remain possible. This observation is consistent with the general notion that protonation of C41 in WT does not induce a large conformational change and may therefore be functionally silent.

Conclusion

The data herein support the pK_a for the genomic HDV ribozyme in the absence of Mg^{2+} as belonging to C75 for WT and to C41 for DM. The observed rate appears to be limited by proton transfer of C75 in the transition state rather than a conformational change or diffusional process. Furthermore, an inverse contribution to the observed isotope effect at high pH supports hydroxide ion as a specific base in a pre-equilibrium step in a multistep reaction mechanism, with water acting as a Brønsted base at neutral and lower pH. Therefore, the inversion of the rate−pH profile for WT upon catalytic divalent ion removal is consistent with a general acid role for C75 in the reaction mechanism in both the absence and presence of Mg^{2+} (GAB model 2). The opposite mechanism in which C75 acts as a general base (GAB model 1) would require the hydroxide ion to serve as a Brønsted acid, which is not chemically tenable.

C75 appears to be the general acid both in the absence *and* presence of Mg^{2+}, which is in agreement with a general acid role for C75 in the presence of Mg^{2+} demonstrated incisively by Das and Piccirilli.[24] The pK_a of C75 in 1 M NaCl and 100 mM EDTA of ~7.5 is nearly identical to its value measured without NaCl extrapolated to no bound Mg^{2+}. This suggests that the local environment for C75 is unchanged upon Mg^{2+} removal and is not appreciably penetrated by bulk monovalent ions, which also agrees with the inability of small molecules to participate in wild-type HDV reactions.[23] The fractionation factor for C75 does not appear to change appreciably either when hydroxide ion catalyzes 2′-OH deprotonation or when a double mutation is made at the structural base quadruple motif. Thus, the catalytic role of C75 in the mechanism is robust. The ability of nucleobases to transfer protons during ribozyme catalysis in the absence of divalent metal ions suggests that RNAs may be capable of catalyzing diverse reactions as envisioned in the origin of life.

Acknowledgment. This work was supported in part by NIH Grant R01-58709, NSF Grant 0527102, and an NSF Graduate Research Fellowship to A.L.C.-S. We thank Vernon Anderson, Durga Chadalavada, Michael Harris, Juliette Lecomte, Shu-ichi Nakano, and Richard Schowen for helpful conversations. We also appreciate the helpful comments of the reviewers.

Supporting Information Available: Derivation and limits of the population-weighted Gross−Butler equation. This material is available free of charge via the Internet at http://pubs.acs.org.

JA801816K